Transformation of Dimetallacyclopentanes into *β*-Substituted Enamine-, Alkylidene-, and α,*β*-Unsaturated Acyl-Bridged Diiron Complexes

Simon Doherty,*,†,‡ Graeme Hogarth,§ Mark R. J. Elsegood,‡ William Clegg,‡ Nicholas H. Rees,‡ and Mark Waugh‡

Department of Chemistry, Bedson Building, The University of Newcastle upon Tyne, Newcastle upon Tyne NE1 7RU, U.K., and Department of Chemistry, University College London, 20 Gordon Street, London WC1H 0AJ, U.K.

Received February 19, 1998

Nucleophilic addition of primary amines RNH_2 to C_β of the diiron allenyl complex $[Fe_2(CO)_6(\mu\text{-}PPh_2)\{\mu-\eta^1:\eta^2\text{-}(H)C{=}C{=}CH_2\}]$ (**1**) affords the zwitterionic dimetallacyclopentane derivatives $[Fe_2(CO)_6(\mu\text{-}PPh_2)\{\mu-\eta^1:\eta^1\text{-}H_2C{-}C(NHR){-}CH_2\}]$ (R = Pr^i (**2a**), CH_2Ph (**2b**), C_6H_{11} (**2c**), Pr^n (**2d**)). In refluxing toluene, **2a**−**d** rearrange to give the nitrogen-coordinated organodiiron α,*β*-unsaturated amines $[Fe_2(CO)_5(\mu\text{-}PPh_2)\{\mu-\eta^1(C):\eta^2(C):\eta^1(N)\text{-}(H)C{=}CCH_3\text{-}(NHR)\}]$ (R = Pr^i (**3a**), CH_2Ph (**3b**), C_6H_{11} (**3c**), Pr^n (**3d**)) via loss of carbon monoxide, a 1,3-hydrogen migration, and coordination of the *β*-amino group. The bridging hydrocarbon in **3a**−**d** adopts a highly unusual exo conformation with respect to the phosphido ligand. Compounds **3a**−**d** are the first diiron *β*-substituted enamine complexes to be isolated and structurally characterized. Such compounds have previously been proposed as short-lived intermediates which readily isomerize to their alkylidene-bridged counterparts. Complexes **3a** and **3c** react with trimethyl phosphite to afford the stable alkylidene valence isomers $[Fe_2(CO)_5\{P(OMe)_3\}(\mu\text{-}PPh_2)\{\mu\text{-}CHC(CH_3)(NHR)\}]$ (R = Pr^i (**4a**), C_6H_{11} (**4c**)). In contrast, in refluxing toluene, **2a**−**b** react with trimethyl phosphite to give the α,*β*-unsaturated bridging acyl complexes $[Fe_2(CO)_5\{P(OMe)_3\}(\mu\text{-}PPh_2)\{\mu\text{-}O{=}C{-}CH{=}CMe(NHR)\}]$ (R = Pr^i (**5a**), CH_2Ph (**5b**)), which probably result from the formal insertion of carbon monoxide into an alkylidene intermediate. Single-crystal X-ray analyses of **5a** and **5b** showed the position of substitution to be the iron atom *σ*-bonded to the acyl oxygen, trans to the phosphido bridge in **5a** and trans to the iron−iron bond in **5b**. Variable-temperature $^{31}P\{^1H\}$ and ^{31}P-^{31}P 2D exchange NMR studies have been used to examine an exchange process that equilibrates two isomers of **4a** and **5b**, which differ in the position of the trimethyl phosphite. At low temperature, **4a** exists as a 4:1 mixture of these two substitutional isomers, while at room temperature they are in fast exchange, on the NMR time scale. The free energy of activation associated with this exchange ($\Delta G^{\ddagger}_{273}$ = 9.5 kcal mol^{-1}, **4a**; $\Delta G^{\ddagger}_{273}$ = 10.4 kcal mol^{-1}, **5b**) is fully consistent with a restricted trigonal twist at the phosphite-substituted iron center. This exchange process also appears to be common to the alkylidene derivative **5b**, which has similar $^{31}P\{^1H\}$ line broadening characteristics and free energy of activation. Full structural details of compounds **2a**, **3a**, **4c**, **5a**, and **5b** are reported.

Introduction

The reactivity of mononuclear complexes of the *σ*−*η*-coordinated allenyl fragment $-C_\alpha(H){=}C_\beta{=}C_\gamma H_2$ has been thoroughly investigated in recent years[1] and found to be dominated by the addition of protic and aprotic nucleophiles to C_β, to give heterosubstituted *π*-allyl derivatives (eq 1)[2] and metallacyclobutenes (eq 2).[3] In contrast, while the η^1-coordinated allenyl fragment appears to be unreactive toward nucleophilic reagents,[4] such complexes readily undergo [2 + 3] cycloaddition reactions with electron-deficient olefins and, in the presence of Lewis acids, carbonyl compounds to give η^1-cyclopentene (eq 3) and η^1-2,5-dihydrofur-3-yl (eq 4)

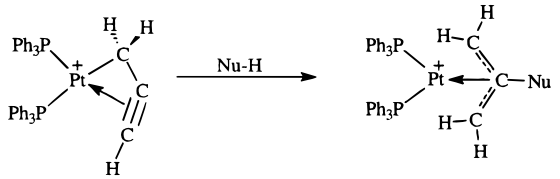

(1)

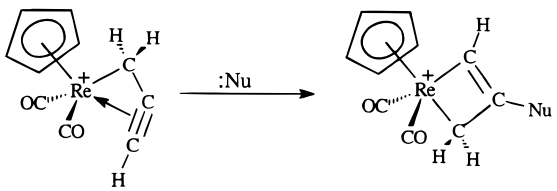

(2)

† E-mail: simon.doherty@newcastle.ac.uk.
‡ University of Newcastle upon Tyne.
§ University College London.

(1) Wojcicki, A. *New J. Chem.* **1994**, *18*, 61. (b) Doherty, S.; Corrigan, J. F.; Carty, A. J.; Sappa, E. *Adv. Organomet. Chem.* **1995**, *37*, 39.

S0276-7333(98)00108-3 CCC: $15.00
Publication on Web 07/03/1998

compounds, respectively.[5] Since the discovery of ratio-

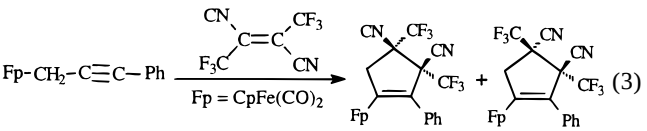

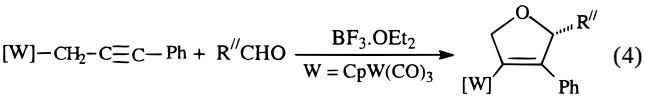

nal, high-yield synthetic routes to binuclear allenyl complexes, which include the addition of diazoalkanes to $\mu-\eta^1:\eta^2$-acetylides,[6] S_N2' attack of a dimetalate at a propargyl halide,[7] and template synthesis,[8] a detailed examination of their reaction chemistry has revealed more disparate and varied reactivity patterns than their mononuclear counterparts. In this regard, examples of unusual coupling reactions[9] (Scheme 1), the addition of nucleophiles to C_α, C_β, and C_γ[10] (Scheme 2), the formation of acyl−allenyl complexes via migratory insertion/elimination of CO into a $\mu-\eta^1:\eta^2$-allenyl ligand (Scheme 3),[11] and the generation of diiron coordinated β,γ-unsaturated amides,[12] esters,[13] and ketones[14] (eq 5) all suggest that the $\sigma-\eta$-coordinated allenyl fragment offers immense potential as a building block for the synthesis

Scheme 1

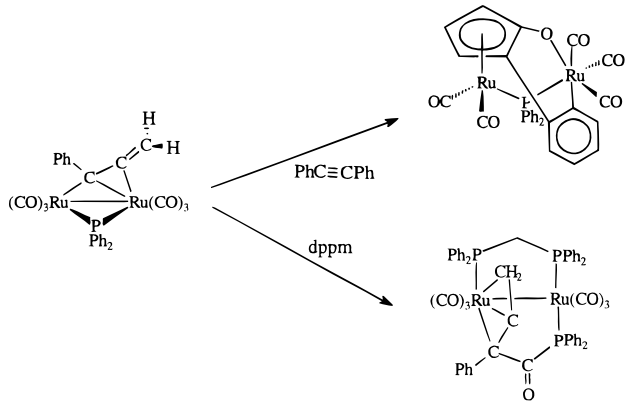

of a wide range of unsaturated organic molecules, provided these products can be liberated from the metal center. Methods currently under investigation include

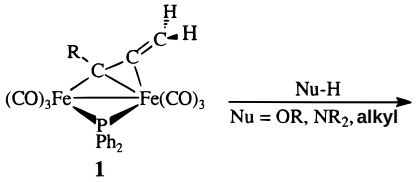

1

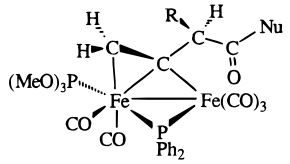

(5)

protonation, oxidative cleavage by Ce(IV), and intramolecular oxidative-addition−reductive-elimination pathways. While we can comfortably draw parallels between the chemistry of mononuclear metal allyl and allenyl complexes, in particular their synthesis and fundamental reactivity patterns, no such comparison can be drawn for their binuclear counterparts, since attempts to isolate the former result in rearrangement to its alkenyl isomer.[15] By analogy with other η^n-coordinated hydrocarbons, we might reasonably expect interaction of the allenyl fragment with a second metal center to enhance its electrophilicity.[16]

Several years ago, Carty and co-workers reported that the reaction chemistry of the binuclear allenyl complex $[Ru_2(CO)_6(\mu\text{-}PPh_2)\{\mu-\eta^1:\eta^2_{\beta,\gamma}\text{-}C(Ph)=C=CH_2\}]$ was dominated by the electrophilic nature of the $\sigma-\eta$-hydrocarbyl

(2) (a) Baize, M.; Blosser, P. W.; Plantevin, V.; Schimpff, D. G.; Gallucci, J. C.; Wojcicki, A. *Organometallics* **1996**, *15*, 164. (b) Plantevin, V.; Blosser, P. W.; Gallucci, J. C.; Wojcicki, A. *Organometallics* **1994**, *13*, 3651. (c) Blosser, P. W.; Schimpff, D. G.; Gallucci, J. C.; Wojcicki, A. *Organometallics* **1993**, *12*, 1992. (d) Hsu, R.-H.; Chen, J.-T.; Lee, G.-H.; Wang, Y. *Organometallics* **1997**, *16*, 1159. (e) Chen, J.-T.; Chen, Y.-K.; Hu, J.-B.; Lee, S.-H.; Wang, Y. *Organometallics* **1997**, *16*, 1476. (f) Huang, T.-M.; Hsu, R.-H.; Yang, C.-S.; Chen, J.-T.; Lee, G.-H.; Wang, Y. *Organometallics* **1994**, *13*, 3657. (g) Huang, T.-M.; Hsu, R.-H.; Yang, C.-S.; Chen, J.-T.; Lee, G.-H.; Wang, Y. *Organometallics* **1994**, *13*, 3577. (h) Chen, C.-C.; Fan, J.-S.; Lee, G.-H.; Peng, S.-M.; Wang, S.-L.; Lui, R.-S. *J. Am. Chem. Soc.* **1995**, *117*, 2933. (i) Huang, T.-M.; Chen, J.-T.; Lee, G.-H.; Wang, Y. *J. Am. Chem. Soc.* **1993**, *115*, 1170. (j) Su, C.-C.; Chen, J.-T.; Lee, G.-H.; Wang, Y. *J. Am. Chem. Soc.* **1994**, *116*, 4999.

(3) Casey, C. P.; Yi, C.-S. *J. Am. Chem. Soc.* **1992**, *114*, 6597.

(4) Huang, T.-M.; Hsu, R.-H.; Yang, C.-S.; Chen, J.-T.; Lee, G.-H.; Wang, Y. *Organometallics* **1994**, *13*, 3657.

(5) For recent examples, see: (a) Tseng, T.-W.; Wu, T.-Y.; Tsai, J.-H.; Lui, Y.-C.; Chen, D.-J.; Lee, G.-H.; Cheng, M.-C.; Wang, Y. *Organometallics* **1994**, *13*, 3963. (b) Shui, H.-G.; Shui, L.-H.; Wang, S.-H.; Wang, S.-L.; Lee, G.-H.; Peng, S.-M.; Lui, R.-S. *J. Am. Chem. Soc.* **1996**, *118*, 530. (c) Wang, S.-H.; Shui, L.-H.; Shui, H.-G.; Liao, Y.-L.; Wang, S.-L.; Lee, G.-H.; Peng, S.-M.; Lui, R.-S. *J. Am. Chem. Soc.* **1994**, *116*, 5967. For a review, see: (d) Welker, M. E. *Chem, Rev.* **1992**, *92*, 97.

(6) (a) Nucciarone, D.; Taylor, N. J.; Carty, A. J. *Organometallics* **1986**, *5*, 1179. (b) Nucciarone, D.; Taylor, N. J.; Carty, A. J. *Organometallics* **1984**, *3*, 177. (c) Nucciarone, D.; MacLaughlin, S. A.; Taylor, N. J.; Carty, A. J. *Organometallics* **1988**, *7*, 106. (d) Blenkiron, P.; Enright, G. D.; Taylor, N. J.; Carty, A. J. *Organometallics* **1996**, *15*, 2855. (e) Carleton, N.; Corrigan, J. F.; Doherty, S.; Pixner, R.; Sun, Y.; Taylor, N. J.; Carty, A. J. *Organometallics* **1994**, *13*, 4179.

(7) (a) Seyferth, D.; Womack, G. B.; Archer, C. M.; Dewan, J. C. *Organometallics* **1989**, *8*, 430. (b) Seyferth, D.; Womack, G. B.; Dewan, J. C. *Organometallics* **1989**, *4*, 398.

(8) Young, G. H.; Wojcicki, A.; Calligaris, M.; Nardin, G.; Brescian-Pahor, N. *J. Am. Chem. Soc.* **1989**, *111*, 6890.

(9) (a) Blenkiron, P.; Breckenridge, S. M.; Taylor, N. J.; Carty, A. J.; Pellinghelli, M. A.; Tiripicchio, A.; Sappa, E. *J. Organomet. Chem.* **1996**, *506*, 229. (b) Ogoshi, S.; Tsutsumi, K.; Ooi, M.; Kurosawa, H. *J. Am. Chem. Soc.* **1995**, *117*, 10415. (c) Ogoshi, S.; Fukunishi, Y.; Tsutsumi, K.; Kurosawa, H. *J. Chem. Soc., Chem. Commun.* **1995**, 2485.

(10) (a) Doherty, S.; Elsegood, M. R. J.; Clegg, W.; Scanlan, T. H.; Rees, N. H. *Chem. Commun.* **1996**, 1545. (b) Meyer, A.; McCabe, D. J.; Curtis, M. D. *Organometallics* **1987**, *6*, 1491. (c) McLain, M. D.; Hay, M. S.; Curtis, M. D.; Kampf, J. W. *Organometallics* **1994**, *13*, 4377. (d) Henrick, K.; McPartlin, M.; Deeming, A. J.; Hasso, S.; Manning, P. *J. Chem. Soc., Dalton Trans.* **1982**, 899. (d) Amouri, H.; Besace, Y.; Vaissermann, J.; Ricard, L. *Organometallics* **1997**, *16*, 2160.

(11) Blenkiron, P.; Corrigan, J. F.; Taylor, N. J.; Carty, A. J.; Doherty, S.; Elsegood, M. R. J.; Clegg, W. *Organometallics* **1997**, *16*, 297.

(12) Doherty, S.; Elsegood, M. R. J.; Clegg, W.; Waugh, M. *Organometallics* **1996**, *15*, 2688.

(13) Doherty, S.; Elsegood, M. R. J.; Clegg, W.; Mampe, D. *Organometallics* **1997**, *16*, 1186.

(14) Doherty, S.; Elsegood, M. R. J.; Clegg, W.; Rees, N. H.; Scanlan, T. H.; Waugh, M. *Organometallics* **1997**, *16*, 3221.

(15) (a) Hogarth, G.; Lavender, M. H. *J. Chem. Soc., Dalton Trans.* **1992**, 2759. (b) Horton, A. D.; Mays, M. J. *J. Chem. Soc., Dalton Trans.* **1990**, 155. (c) Hay, C. M.; Horton, A. D.; Mays, M. J.; Raithby, P. R. *Polyhedron* **1988**, *7*, 987.

(16) Fatiadi, A. J. J. *Res. Natl. Inst. Stand. Technol.* **1991**, *96*, 1. (b) Kerber, R. C. In *Comprehensive Organometallic Chemistry*; Wilkinson, G., Stone. F. G. A., Eds.; Pergamon Press: Oxford, 1994: Vol. 7, pp 102−229. Bates, R. W. *Ibid*. Vol. 12, pp 349−386. Fagan, P. J. *Ibid*. Vol. 3, pp 231−258.

Scheme 2

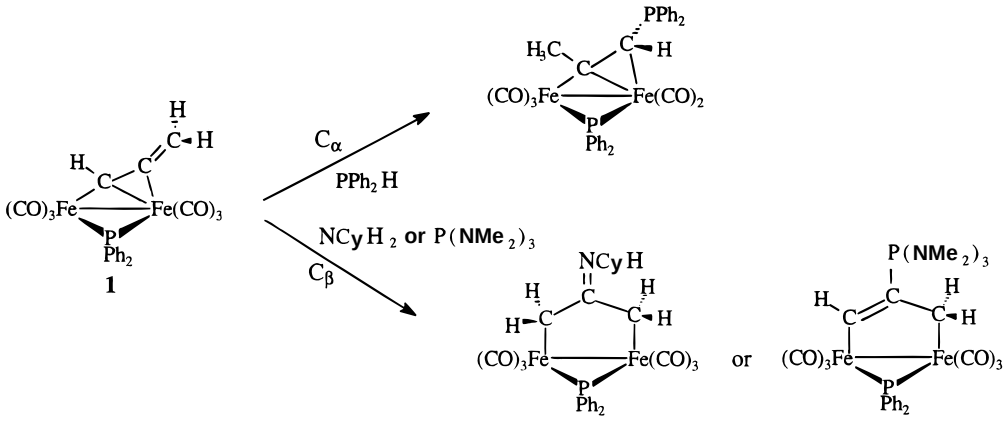

Scheme 3

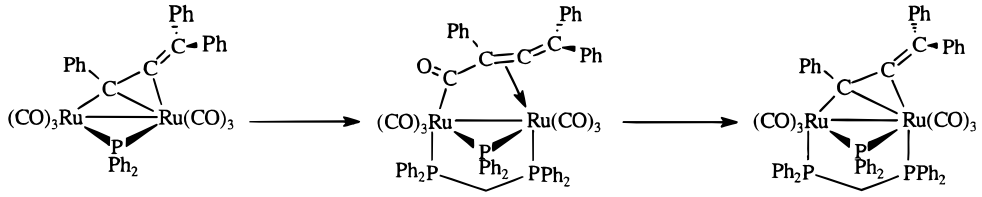

fragment.[17] In particular, protic nitrogen-based nucleophiles add to C_β, with 1,3-hydrogen migration to C_α, to afford the dimetallacyclopentane derivatives $[Ru_2(CO)_6(\mu\text{-}PPh_2)\{\mu-\eta^1:\eta^1\text{-}PhHC-C(NHR)-CH_2\}]$ while neutral phosphorus- and carbon-based nucleophiles gave the dimetallacyclopentene derivatives $[Ru_2(CO)_6(\mu\text{-}PPh_2)\{\mu-\eta^1:\eta^1\text{-}PhC=C(Nu)-CH_2\}]$. We have recently succeeded in preparing the corresponding diiron allenyl complex $[Fe_2(CO)_6(\mu\text{-}PPh_2)\{\mu-\eta^1:\eta^2_{\alpha,\beta}\text{-}C(H)=C=CH_2\}]$ (**1**) and begun to conduct a systematic examination of its reaction chemistry to compare with that reported by Carty. We too have found that selected nitrogen-based nucleophiles add regiospecifically to C_β. However, a number of alternative reaction pathways have also been identified including regiospecific attack of phosphorus-based nucleophiles at C_α to afford $\mu-\eta^1:\eta^2$-phosphino alkenyl complexes (Scheme 2)[18] and the generation of novel organodiiron coordinated β,γ-unsaturated ketones and esters (eq 5) via carbonyl−allenyl−nucleophile coupling. Herein, we report that the dimetallacyclopentane derivatives $[Fe_2(CO)_6(\mu\text{-}PPh_2)\{\mu-\eta^1:\eta^1\text{-}H_2C-C(NHR)-CH_2\}]$ that result from nucleophilic addition of primary amines to C_β of the binuclear allenyl complex $[Fe_2(CO)_6(\mu\text{-}PPh_2)\{\mu-\eta^1:\eta^2_{\alpha,\beta}\text{-}C(H)=C=CH_2\}]$ (**1**) readily undergo a 1,3-hydrogen migration to afford the novel organodiiron coordinated α,β-unsaturated amines $[Fe_2(CO)_5(\mu\text{-}PPh_2)\{\mu-\eta^1(C):\eta^2(C):\eta^1(N)\text{-}(H)C=CCH_3(NHR)\}]$. These are the first examples of stable diiron β-substituted enamine complexes to be isolated and structurally characterized. Previously, such compounds have been proposed as short-lived intermediates in the addition of RNH_2 across the multiple bond of the acetylide complexes $[Fe_2(CO)_6(\mu\text{-}PPh_2)\{\mu-\eta^1:\eta^2\text{-}C\equiv CR\}]$, which subsequently rearrange to give the more stable alkylidene coordination isomers.[19]

(17) Breckenridge, S. M.; Taylor, N. J.; Carty, A. J. *Organometallics* **1991**, *10*, 837.

(18) Doherty, S.; Elsegood, M. R. J.; Clegg, W.; Mampe, D.; Rees, N. H. *Organometallics* **1996**, *15*, 5302.

Results and Discussion

Synthesis of Dimetallacyclopentane Derivatives 2a−d. Solutions of **1** and primary amines RNH_2 (R = Pr^i, CH_2Ph, C_6H_{11}, Pr^n) in diethyl ether gradually turn orange over 24 h to afford the zwitterionic dimetallacyclopentane derivatives $[Fe_2(CO)_6(\mu\text{-}PPh_2)\{\mu-\eta^1:\eta^1\text{-}H_2C-C(NHR)-CH_2\}]$ (R = Pr^i (**2a**), CH_2Ph (**2b**), C_6H_{11} (**2c**), Pr^n (**2d**)), isolated as yellow crystalline solids in yields of up to 80% (eq 6). In each case, reaction monitoring by IR spectroscopy and thin-layer chromatography showed only the formation **2a−d** with no evidence for the organodiiron-coordinated β,γ-unsaturated esters $[Fe_2(CO)_5(\mu\text{-}PPh_2)(\mu-\eta^1(O):\eta^1(C):\eta^2(C)\text{-}\{(NRH)C(O)CH_2\}C=CH_2)]$ (see eq 5), previously isolated from the reaction between **1** and *tert*-butylamine (R = Bu^t).[12] Overall, the formation of **2a** requires nucleophilic addition of isopropylamine to the central allenylic carbon in **1** and proton transfer to C_α, possibly via an intermediate zwitterionic enamine such as (**Ia**), and a subsequent 1,3-shift of iron from C_α to C_γ and of an N-bound hydrogen to C_α (Scheme 4). In an attempt to isolate an intermediate enamine complex, a diethyl ether solution of **1** was treated with triethylamine. Unfortunately, there was no evidence of reaction, even after stirring for 48 h at room temperature, a far longer time than generally required for **1** to react with nitrogen-, oxygen-, and phosphorus-based nucleophiles. Since the reaction mixture contains excess base, we have not excluded the possibility that **2** could form via a protonation−deprotonation pathway, i.e., an intermolecular process involving an intermediate of type (**Ib**).

The ^1H and $^{13}C\{^1H\}$ NMR spectroscopic features of **2a−d** are fully consistent with the proposed dimetal-

(19) (a) Mott, G. M.; Carty, A. J. *Inorg, Chem.* **1983**, *22*, 2726. (b) Carty, A. J.; Mott, G. N.; Taylor, N. J.; Yule, J. E. *J. Am. Chem. Soc.* **1978**, *100*, 3051. (c) Cherkas, A. A.; Randall, L. H.; Taylor, N. J.; Mott, G. N.; Yule, J. E.; Guinamant, J. L.; Carty, A. J. *Oganometallics* **1990**, *9*, 1677. (d) Cherkas, A. A.; Mott, G. N.; Granby, R.; MacLaughlin, S. A.; Yule, J. E.; Taylor, N. J.; Carty, A. J. *Organometallics* **1988**, *7*, 1115.

Scheme 4

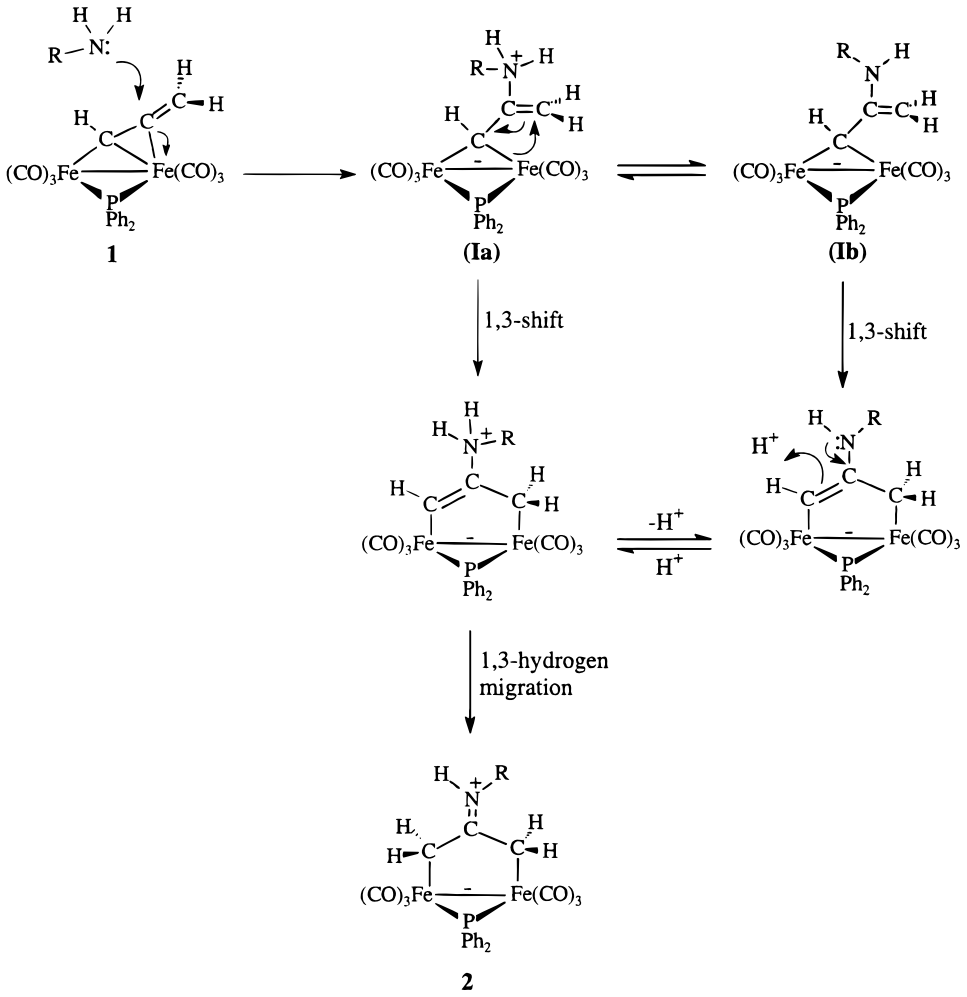

lacyclic structure. In the ^{1}H NMR spectrum, four distinct high-field resonances between δ 1.25−0.74 ppm are characteristic of protons attached to C_α and C_γ of a five-membered dimetallacycle. In each case, the assignment of these signals has been confirmed with ^{13}C−^{1}H single-bond correlation studies. The presence of four distinct signals associated with C_α and C_γ suggests that rotation about the C═N imine bond is slow on the NMR time scale. The ^{13}C{^{1}H} NMR signals associated with C_α and C_γ appear between δ 8.0 and 10.8 ppm, similar to values previously reported for zwitterionic dimetallacyclopentane complexes.[17] The resonance associated with C_β appears as a weak signal in the low-field region and indicates a significant contribution from its imine resonance structure. The resonances belonging to the carbonyl ligands appear as broad undefined signals between δ 211 and 217, which suggests the onset of trigonal rotation at room temperature. In marked contrast, the ^{13}C{^{1}H} NMR spectra of their ruthenium counterparts contains six distinct carbonyl signals. Although these spectroscopic characteristics are a reliable probe of structure and bonding,[20] a single-crystal X-ray analysis of **2a** was undertaken to provide precise structural details.

X-ray Structure of [$Fe_2(CO)_6(\mu$-$PPh_2)\{\mu-\eta^1:\eta^1$-$H_2C-C(NHPr^i)-CH_2\}$] (2a). The molecular structure of **2a** is shown in Figure 1 and a selection of relevant bond lengths and angles listed in Table 1. The dimetallacyclopentane structure adopts a folded envelope conformation with the C_3 flap located exo to the phosphido bridge to avoid unfavorable steric interactions. The two iron atoms both support three mutually cis

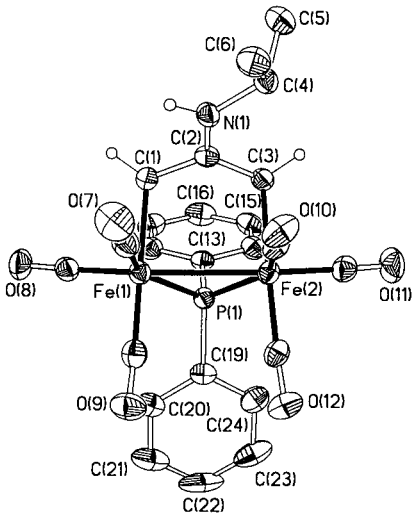

Figure 1. Molecular structure of [$Fe_2(CO)_6(\mu$-$PPh_2)\{\mu-\eta^1:\eta^1$-$H_2C-C(NHPr^i)-CH_2\}$] (**2a**). Phenyl and isopropyl hydrogen atoms have been omitted. Carbonyl carbons have the same numbers as the oxygen atoms. Ellipsoids are at the 50% probability level.

(20) Cherkas, A. A.; Breckenridge, S. M.; Carty, A. J. *Polyhedron* **1992**, *11*, 1075.

Table 1. Selected Bond Distances (Å) and Angles (deg) for Compound 2a

Fe(1)-Fe(2)	2.7413(4)	Fe(1)−C(1)	2.114(2)
Fe(2)−C(3)	2.128(2)	C(1)−C(2)	1.463(3)
C(2)−C(3)	1.440(3)	C(2)−N(1)	1.325(3)
N(1)−C(4)	1.471(3)	Fe(1)−P(1)	2.2164(6)
Fe(2)−P(1)	2.2089(6)	Fe(1)−C(7)	1.806(2)
Fe(1)−C(8)	1.758(2)	Fe(1)−C(9)	1.799(2)
Fe(2)−C(10)	1.797(2)	Fe(2)−C(11)	1.784(2)
Fe(2)−C(12)	1.787(2)		
C(1)−C(2)−C(3)	119.22(18)	C(1)−C(2)−N(1)	118.50(19)
C(3)−C(2)−N(1)	122.24(19)	Fe(1)−P(1)−Fe(2)	76.56(2)

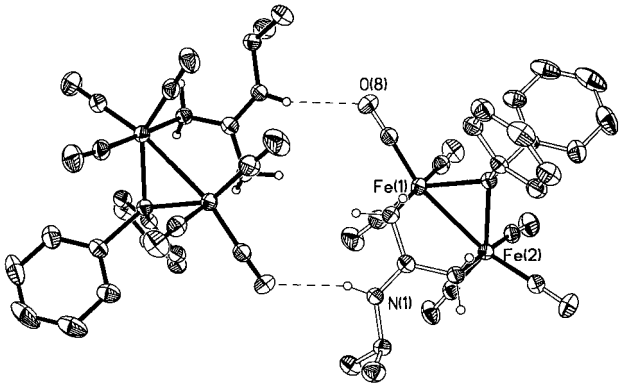

Figure 2. Dimer of $[Fe_2(CO)_6(\mu\text{-}PPh_2)\{\mu\text{−}\eta^1\text{:}\eta^1\text{-}H_2C\text{−}C(N\text{-}HPr^i)\text{−}CH_2\}]$ (**2a**) showing the intermolecular N−H- - -O(carbonyl) hydrogen bonding interactions.

terminal carbonyl ligands which are eclipsed with respect to each other, presumably constrained by the rigid three-carbon hydrocarbyl bridging ligand. The C_3 hydrocarbyl ligand symmetrically bridges the two iron atoms σ-bonded to Fe(1) and Fe(2) [Fe(1)−C(1) = 2.114(2) Å; Fe(2)−C(3) = 2.128(2) Å], and the carbon−carbon bond lengths [C(1)−C(2) = 1.463(3) Å, C(2)−C(3) = 1.440(3) Å] within the metallacyclic structure are comparable to values previously reported for $C(sp^2)-C(sp^3)$ single bonds in other metallacycles. The short N(1)−C(2) bond length (1.325(3) Å) and the planar nature of N(1) (assumed in the constrained refinement of the H atoms after it was found in an appropriate position in a difference map) and C(2) (sum of angles = 359.96°) are characteristic of **2a** having substantial imine character.[12,17] Interestingly, individual diiron fragments are associated through intermolecular H-bonding interactions between the imine N−H and the oxygen atom of a carbonyl group on a neighboring diiron unit (N- - -O = 3.166 Å and an N−H- - -O angle of 150°) to form centrosymmetric dimers. These hydrogen-bond interactions do not propagate through the crystal but are confined to individual dimeric units, as shown in Figure 2. Braga and co-workers have used the Cambridge Structural Database to undertake a systematic examination of hydrogen-bond patterns in organometallic crystals and noted that CO ligands can behave as hydrogen-bond acceptors from donors such as O−H, N−H, and even C−H.[21] The hydrogen-bonding parameters in **2a**, in particular the N−H- - -O angle of 150°,

Scheme 5

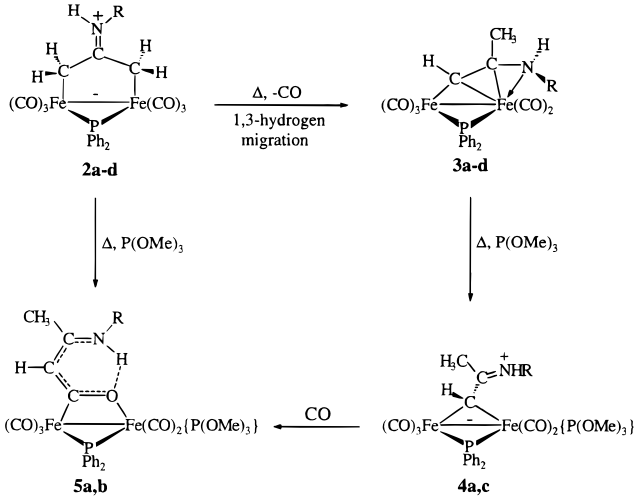

are consistent with oxygen lone pair density in a "ketonic" direction, as previously described for terminal carbonyl ligands in a range of first-row transition-metal organometallic compounds.

Thermal Decarbonylation of 2a−d. Surprisingly, upon standing, *n*-hexane solutions of **2a−d** smoothly decarbonylate over several weeks to afford $[Fe_2(CO)_5(\mu\text{-}PPh_2)\{\mu\text{−}\eta^1(C)\text{:}\eta^2(C)\text{:}\eta^1(N)\text{-}(H)C{=}CCH_3(NHR)\}]$ (R = Pr^i (**3a**), CH_2Ph (**3b**), C_6H_{11} (**3c**), Pr^n (**3d**)), a transformation that occurs quantitatively and more rapidly (3−5 h) in refluxing toluene (Scheme 5). In the ^1H NMR spectrum, doublet resonances between δ 4.70 and 4.90 (J_{PH} = 20.5 Hz) and δ 2.39 and 2.40 indicate the presence of a bridging vinyl ligand. The former resonance belongs to the proton attached to C_α of the $\sigma\text{−}\eta$-alkenyl ligand and is unusually high-field shifted; such protons generally appear at much lower field in the region δ 6.0−8.9 ppm. We also note that $^3J_{PH}$ is significantly larger than previously reported values which typically range from 3.7 to 5.9 Hz.[23] The spectroscopic assignment of $C_\alpha\text{−}H$ has been confirmed by $^{13}C\text{−}^1H$ single-bond correlation studies, which show that C_α of the bridging vinyl ligand appears as a downfield signal between δ 127−128 ($^2J_{PC}$ = 40.3 Hz). The unusual ^1H NMR spectroscopic characteristics of **3a−d** are believed to reflect the unconventional bonding arrangement of the β-amino−alkenyl ligand, which adopts an exo conformation with respect to the phosphido bridge rather than the more familiar endo geometry (vide infra).[23] On the basis of these apparent differences, we might expect the chemical shift of vinyl protons together with the magnitude of $^3J_{PH}$ to provide a reliable first indication of the conformation of phosphido-bridged alkenyl complexes. In the carbonyl region, three separate resonances, two doublets between δ 210 and 220, each corresponding to one carbonyl, and a sharp doublet at approximately δ 214 associated with the three carbonyls of the $Fe(CO)_3$ fragment, reveal that $\sigma\text{−}\eta$-vinyl fluxionality[23b,24] is slow at room temperature.

(21) (a) Biradha, K.; Desiraju, G. R.; Braga, D.; Grepioni, F. *Organometallics* **1996**, *15*, 1285. (b) Braga, D.; Grepioni, F. *Chem. Commun*. **1996**, 571. (c) Braga, D.; Grepioni, F.; Biradha, K.; Pedireddi, V. R.; Desiraju, G. R. *J. Am. Chem. Soc*. **1995**, *117*, 3156.

(22) (a) MacLaughlin, S. A.; Doherty, S.; Taylor, N. J.; Carty, A. J. *Organometallics* **1992**, *11*, 4315. (b) Hogarth, G.; Lavender, M. H. *J. Chem. Soc., Dalton Trans*. **1994**, 3389.

(23) Breckenridge, S. M.; MacLaughlin, S. A.; Taylor, N. J.; Carty, A. J. *J. Chem. Soc., Chem. Commun*. **1991**, 1718. (b) Xue, Z.; Sieber, W. J.; Knobler, C. B.; Kaesz, H. D. *J. Am. Chem. Soc*. **1990**, *112*, 1825. (c) Kaesz, H. D.; Xue, Z.; Chen, Y.-J.; Knobler, C. B.; Krone-Schmidt, W.; Sieber, W. J.; Boag, N. M. *Pure Appl. Chem*. **1988**, *60*, 1245. (e) Boothman, J.; Hogarth, G. *J. Organomet. Chem*. **1992**, *437*, 201.

This is perhaps not surprising as complexes **3a**−**d** can most aptly be considered as amino-tethered $\sigma-\eta$-alkenyl complexes and as such are unlikely to undergo site exchange via the windshield-wiper mechanism (Scheme 6). Such an exchange would also require cleavage of the anchoring metal−amino interaction and internuclear migration of a carbonyl ligand. The doublet resonance at δ 214 corresponds to three CO's which are interconverting on the NMR time scale, most likely via trigonal rotation. Such behavior is common in binuclear complexes.

Scheme 6

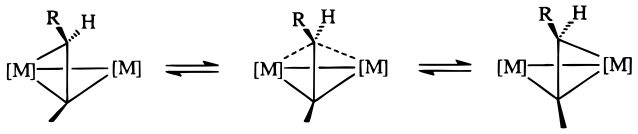

Carty and co-workers have previously reported[19] that primary amines $R'NH_2$ react with the $\sigma-\eta$-acetylide complexes $[Fe_2(CO)_6(\mu\text{-}PPh_2)\{\mu-\eta^1:\eta^2\text{-}C{\equiv}CR\}]$ to give either a one carbon-bridged zwitterionic alkylidene complex (**IV**) or a two carbon-bridged 2-amino-1-metallaphenethylidene complex (**V**), formal valence isomers of the β- and α-amino-substituted alkenyl complexes **II** and **III** respectively (Scheme 7). Variable-temperature NMR studies have shown that **IV** forms via the μ-vinylidene intermediate $[Fe_2(CO)_6(\mu\text{-}PPh_2)\{\mu-\eta^1:\eta^1\text{-}C{=}C(R)NR'H_2\}]$ without any evidence for the expected β-substituted enamine $[Fe_2(CO)_6(\mu\text{-}PPh_2)\{\mu-\eta^1:\eta^2\text{-}C(H){=}C(R)NR'H\}]$ (**II**). In contrast, formation of **V** involves nucleophilic addition to C_α to give a short-lived ammonium intermediate, which undergoes proton transfer to afford a longer-lived, spectroscopically characterized, α-substituted enamine $[Fe_2(CO)_6(\mu\text{-}PPh_2)\{\mu-\eta^1:\eta^2\text{-}C(NR'H){=}C(R)H\}]$ (**III**), which subsequently rearranges to the thermodynamically more stable valence isomer **V**. Although these addition reactions most likely involve α- and β-substituted enamine intermediates, only the former has been spectroscopically characterized and no such compounds have yet been structurally characterized. Compounds **3a**−**d** are the first diiron β-substituted enamine complexes to be isolated and crystallographically characterized (vide infra). Presumably, coordination of the β-amino group stabilizes these compounds with respect to rearrangement to their alkylidene valence isomers.

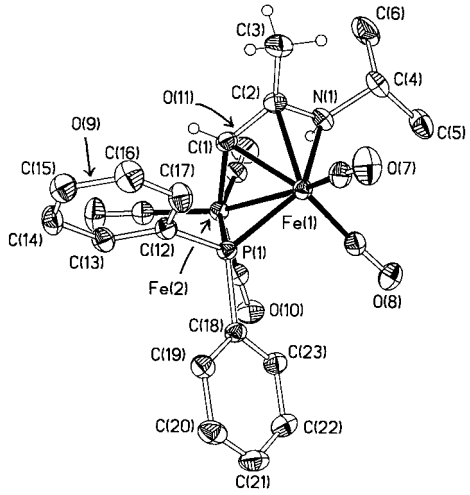

Figure 3. Molecular structure of $[Fe_2(CO)_5(\mu\text{-}PPh_2)\{\mu-\eta^1(C):\eta^2(C):\eta^1(N)\text{-}CH{=}CCH_3(NHPr^i)\}]$ (**3a**). Phenyl and isopropyl hydrogen atoms have been omitted. Carbonyl carbons have the same numbers as the oxygen atoms. Ellipsoids are at the 50% probability level.

X-ray Crystal Structure of $[Fe_2(CO)_5(\mu\text{-}PPh_2)\{\mu-\eta^1(C):\eta^2(C):\eta^1(N)\text{-}(H)C{=}CCH_3(NHPr^i)\}]$ (3a). The unusual nature of this transformation prompted a single-crystal X-ray structure determination of **3a** to establish the precise nature of the bridging hydrocarbyl ligand, its conformation with respect to the phosphido bridge, and coordination to the diiron fragment. A perspective view of the molecular structure together with the atomic-numbering scheme is shown in Figure 3, and a selection of bond distances and angles is listed in Table 2. Overall, the formation of **3a** requires a 1,3-hydrogen migration to convert the C_3-bridging hydrocarbon into the β-isopropylamino-substituted alkenyl ligand, loss of carbon monoxide, and coordination of the β-amino group. The most noteworthy feature of this structure is the unusual $\sigma-\eta$-coordinated α,β-unsaturated amine, more aptly described as a β-substituted enamine. Complex **3a** is a rare example of a β-disub-

Scheme 7

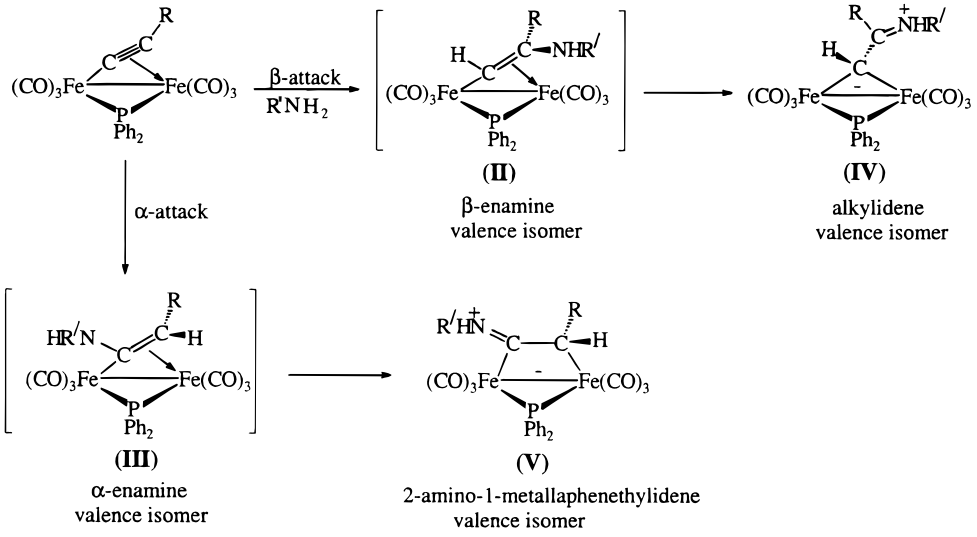

Table 2. Selected Bond Distances (Å) and Angles (deg) for Compound 3a

Fe(1)−Fe(2)	2.5723(5)	Fe(1)−C(1)	2.069(2)
Fe(1)−C(2)	2.073(2)	Fe(1)−N(1)	2.059(2)
Fe(2)−C(1)	1.993(2)	Fe(1)−P(1)	2.1813(7)
Fe(2)−P(1)	2.2317(7)	Fe(1)−C(7)	1.775(3)
Fe(1)−C(8)	1.777(3)	Fe(2)−C(9)	1.801(3)
Fe(2)−C(10)	1.788(3)	Fe(2)−C(11)	1.791(1)
C(1)−C(2)	1.395(3)	C(2)−C(3)	1.508(4)
C(2)−N(1)	1.412(3)		
Fe(1)−P(1)−Fe(2)	71.30(2)	C(1)−C(2)−C(3)	124.5(2)
C(3)−C(2)−N(1)	120.7(2)	P(1)−Fe(1)−N(1)	140.23(6)
C(1)−C(2)−N(1)	114.7(2)		

stituted μ-alkenyl-bridged diiron complex. The two iron atoms are bridged by the new hydrocarbyl fragment in the familiar $\sigma-\eta$ mode with the α-carbon, C(1), bound somewhat asymmetrically to both iron atoms [Fe(2)−C(1) = 1.993(2) Å, Fe(1)−C(1) = 2.069(2) Å] and the β-carbon, C(2), attached to only one metal center [Fe(1)−C(2) = 2.073(2) Å]. A large number of $\sigma-\eta$-alkenyl complexes have been structurally characterized, and a comparison of Fe−C_α and Fe−C_β bond lengths reveals some noteworthy differences. First, Fe(1)−C(2) is substantially shorter than previously reported values which generally lie in the range 2.141−2.286 Å. Second, the Fe(1)−C(1) bond length is slightly shorter than expected, based on values for other β-substituted alkenyl complexes. Interestingly, the β-isopropylamino group coordinates to Fe(2) and occupies a site approximately trans to P(1) [∠P(1)−Fe(1)−N(1) = 140.23(6)°] to form a three-membered FeNC ring. One of the iron atoms, Fe(2), supports three terminally bound carbonyls, one trans to the metal−metal bond, one trans to the phosphido bridge, and the remaining one trans to the bridging hydrocarbyl ligand. The other iron atom, Fe(1), carries two carbonyls, one trans to the metal−metal bond the other trans to the alkenyl bridge, while the β-amino group occupies the site trans to the bridging phosphido ligand. The C(1)−C(2) bond length [1.395(3) Å] shows the elongation expected upon η^2-coordination to a metal center and is comparable to values in other phosphido-bridged diiron alkenyl complexes. The C(2)−N(1) bond length [1.412(3) Å] is close to that expected for a C−N single bond and further reinforces our description of **3a** as an enamine-bridged diiron complex, which is prevented from existing in its alkylidene form due to coordination of the β-amino group. Surprisingly, the $\sigma-\eta$-alkenyl ligand in **3a** adopts an exo conformation, that is the α-carbon of the alkenyl ligand is orientated toward the phosphido bridge. In contrast, $\sigma-\eta$-diiron alkenyl complexes generally adopt endo conformations in which the α-substituted carbon is orientated away from the phosphido bridge to avoid unfavorable steric interactions.

The most common route to alkenyl-bridged diiron complexes is the addition of a binuclear hydride to the carbon−carbon triple bond of an alkyne.[26] Terminal alkynes generally react with a high regioselectivity for Markovnikov addition to afford the cis-α-substituted isomer, in which the alkenyl ligand adopts an endo conformation. The product of an anti-Markovnikov addition is a β-substituted alkenyl, which, for cis addition, orientates the β-substituent away from the phosphido bridge, again to limit unfavorable steric interactions, i.e., β-substituted alkenyl complexes also prefer to exist as endo conformers. Similarly, hydrodimetalation of internal alkynes generally gives the endo isomer, again the presence of a bulky α-substituent and the orientation of the β-substituent away from the phosphido bridge ensures that the endo conformer is dominant. On the basis of these observations, it is not surprising that **3a**, which contains a β-disubstituted, α-unsubstituted alkenyl ligand, adopts the less familiar exo conformation, first to minimize steric interactions between the substituents on the β-disubstituted carbon and the phosphido bridge and second coordination of the β-isopropyl amino group necessarily constrains the alkenyl ligand in an endo conformation.

Overall, the formation of **3** requires a 1,3-hydrogen migration (Scheme 8) via one of two possible pathways, the first of which is entirely intramolecular and involves loss of carbon monoxide, oxidative addition of a C−H bond of the dimetallacyclopentane to give an unsaturated hydride-bridged intermediate (**VIa**), stabilized by a contribution from the carbene resonance form (**VIb**). A 1,3-shift of the iron, or valence isomerization to (**VII**), followed by reductive elimination of the metal−hydride and coordination of the amino group would give **3**. In contrast, pathway b involves reversible formation of the ammonium-substituted dimetallacyclopentene intermediate (**IX**) and requires that a hydrogen of the methyl group of **3** must come from an exchangeable proton source. To distinguish these two pathways the conversion of **2** into **3** was carried out in the presence of a large excess of ethanol-d_1. The ^{2}H NMR spectrum of the product isolated under these conditions showed that there was no deuterium incorporation into the methyl substituent. Thus, at this stage, we favor the oxidative-addition reductive-elimination sequence since the electron-rich FePFe framework of the zwitterionic dimetallacyclopentane is likely to favor oxidative addition of a C−H bond. The formal increase in electron count associated with this step readily accounts for the loss of CO, while the subsequent product-forming reductive elimination generates the vacant coordination site that is eventually occupied by the β-amino substituent, via an intermediate alkylidene-bridged complex. In contrast, the second pathway involves the reversible formation of intermediate **IX** and does not require net loss of CO. Moreover, if **IX** was an intermediate, we might expect to obtain the unsubstituted complex [$Fe_2(CO)_6$-(μ-PPh_2){$\mu-\eta^1$:η^2-(*H*)C═CCH_3(NHR)}] as a byproduct in the formation of **2**. We have found no evidence for the formation of such a compound either during the preparation of **2a**−**d** or its transformation into **3a**−**d**. Thus, it appears that dissociation is integral to the hydride migration step.

Dimetallacyclopentane complexes are relatively rare,[27] and their transformation into $\sigma-\eta$-alkenyl complexes via a 1,3-hydrogen migration is unprecedented. However, we note that allene reacts with the bimetallic

(24) Shapley, J. R.; Richter, S. I.; Tachikawa, M.; Keister, J. B. *J. Organomet. Chem.* **1975**, *94*, C43. (b) Farrugia, L.; Chi, Y.; Tu, W.-C. *Organometallics* **1993**, *12*, 1616 and references therein.

(25) (a) Hogarth, G.; Lavender, M. H.; Shukri, K. *Organometallics* **1995**, *14*, 2325. (b) Orpen, A. G. *J. Chem. Soc., Dalton Trans.* **1983**, 1427.

(26) (a) Conole, G.; Henrick, K.; McPartlin, M.; Horton, A. D.; Mays, M. J. *New J. Chem.* **1988**, *12*, 559. (b) Horton, A. D.; Kemball, A. C.; Mays, M. J. *J. Chem. Soc., Dalton Trans.* **1988**, 2953. (c) Graff, J. L.; Wrighton, M. S. *J. Am. Chem. Soc.* **1980**, *102*, 2123.

Scheme 8

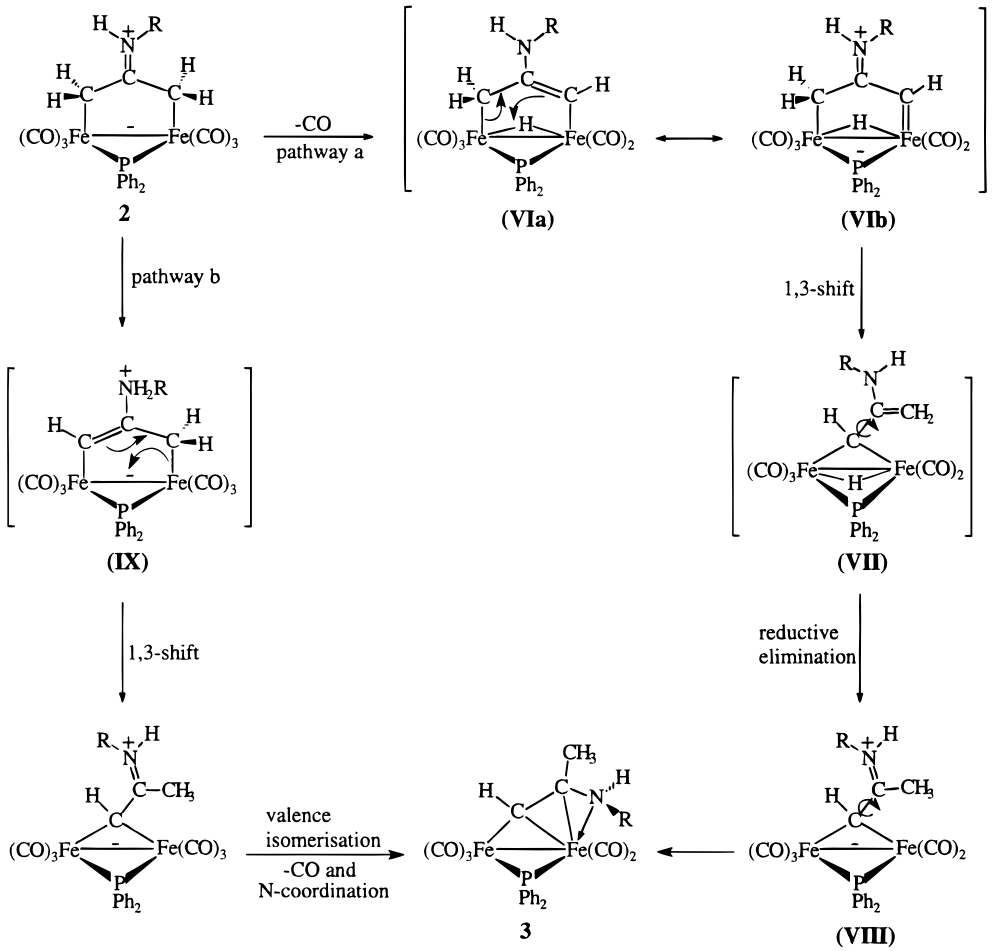

hydride $[Fe_2(CO)_4(\mu\text{-H})(\mu\text{-CO})(\mu\text{-PPh}_2)(\mu\text{-dppm})]$ to afford the $\sigma-\eta$-alkenyl complex $[Fe_2(CO)_4\{\mu-\eta^1{:}\eta^2\text{-HC=CH(CH}_3)\}(\mu\text{-PPh}_2)(\mu\text{-dppm})]$, possibly via a fleeting intermediary dimetallacyclopentane[15a] that readily undergoes a facile 1,3-hydrogen migration. In contrast, dimetallacyclopentenones are more common and generally result from alkyne−CO coupling and their transformation into $\sigma-\eta$-alkenyl complexes, usually via protonation, is well documented, although a number of different mechanisms have been suggested.[27e,h,i]

Formation of μ-Alkylidene Derivatives $[Fe_2(CO)_5\{P(OMe)_3\}(\mu\text{-PPh}_2)\{\mu\text{-O=C−CH=CMe(NHR)}\}]$. Assuming the stability of the coordinated enamine liagand in **3a**, with respect to its μ-alkylidene valence form, arises from coordination of the β-amino group, we reasoned that substitution of the Fe−N interaction with trimethyl phosphite would result in rearrangement to give the dipolar μ-alkylidene derivative $[Fe_2(CO)_5\{P(OMe)_3\}(\mu\text{-PPh}_2)(\mu\text{-CHC(CH}_3)\{NHPr^i\})]$ (**4a**). Note, our discussion in terms of valence isomers refers solely to the nature of the coordinated ligand. Thermolysis of a toluene solution of **3a** results in a gradual color change from orange to red and quantitative formation of $[Fe_2(CO)_5\{P(OMe)_3\}(\mu\text{-PPh}_2)(\mu\text{-CHC(CH}_3)\{NHPr^i\})]$ (**4a**) (Scheme 5), as evidenced from TLC and IR spectroscopy, although isolated yields were closer to 70%. In the $^{31}P\{^1H\}$ NMR spectrum of **4a**, two doublets (δ 187.4, 146.0; $^2J_{PP}$ = 44.5 Hz) confirm the presence of a phosphido bridge and a metal-bound trimethyl phosphite ligand. Interestingly, the high-field resonance appears as an exchange-broadened signal while the one at lower field is relatively sharp. The magnitude of $^2J_{PP}$ (44.5 Hz) strongly suggests that the phosphido bridge and trimethyl phosphite are mutually cis. A minor set of doublets in the $^{31}P\{^1H\}$ NMR spectrum [●, major endo isomer; △, minor exo isomer; ◊ impurity, Figure 7] is thought to correspond to an isomer in which the alkylidene C−H is orientated exo with respect to the phosphido bridge. Such an isomer would experience unfavorable steric interactions between the remaining alkylidene substituent and the phosphido bridging group. In the ^1H NMR spectra of **4a**, a high-field doublet of doublets at δ 1.46 ($^3J_{PH}$ = 34.8, 3.2 Hz) is characteristic of a proton attached to a one-carbon bridging alkylidene carbon. This assignment has been further supported by a $^{13}C-^1H$ heteronuclear single-

(27) For dimetallcyclopentanes, see: (a) Theopold, K. H.; Bergman, R. G. *J. Am. Chem. Soc.* **1980**, 102, 5694. (b) Theopold, K. H.; Bergman, R. G. *Organometallics* **1982**, *1*, 1571. (c) Motyl, K. M.; Norton, J. R.; Schauer, C. K.; Anderson, O. P. *J. Am. Chem. Soc.* **1982**, *102*, 7325. For dimetallacyclopentenones, see: (e) Dyke, A. F.; Knox, S. A. R.; Morris, M. J.; Naish, P. J. *J. Chem. Soc., Dalton Trans.* **1983**, 1417. (f) Burn, M. J.; Kiel, G.-Y.; Seils, F.; Takats, J.; Washington, J. *J. Am. Chem. Soc.* **1989**, *111*, 6850. (g) Dyke, A. F.; Knox, S. A. R.; Naish, P. J.; Taylor, G. E. *J. Chem. Soc., Dalton Trans.* **1982**, 1297. (h) Miraz, H. A.; Jagadese, J. V.; Puddephatt, R. J. *Organometallics* **1994**, *13*, 3063. (i) Casey, C. P.; Carino, R. S.; Sakaba, H. *Organometallics* **1997**, *16*, 419. (j) Johnson, K. A.; Vashon, M. D.; Moasser, B.; Warmka, B. K.; Gladfelter, W. L. *Organometallics* **1995**, *14*, 461. (k) Johnson, K. A.; Gladfelter, W. L. *Organometallics* **1992**, *11*, 2534. (l) Gracey, B. P.; Knox, S. A. R.; Macpherson, K. A.; Orpen, A. G.; Stobart, S. R. *J. Chem. Soc., Dalton Trans.* **1985**, 1935.

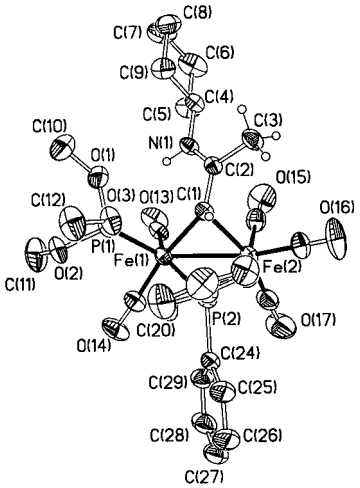

Figure 4. Molecular structure of $[Fe_2(CO)_5\{P(OMe)_3\}(\mu\text{-}PPh_2)(\mu\text{-}CHC(CH_3)\{NHCy\})]$ (**4c**). Phenyl, cyclohexyl, and phosphite methyl hydrogen atoms have been omitted. Carbonyl carbons have the same numbers as the oxygen atoms. Ellipsoids are at the 50% probability level.

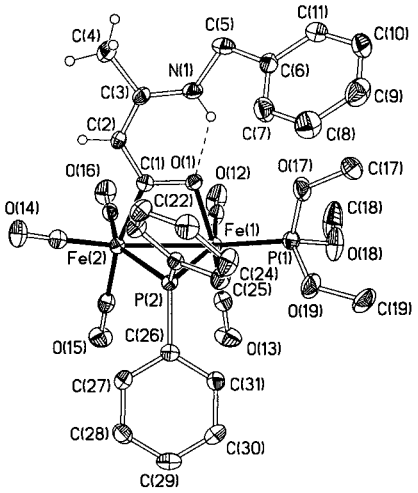

Figure 6. Molecular structure of $[Fe_2(CO)_5\{P(OMe)_3\}(\mu\text{-}PPh_2)\{\mu\text{-}O{=}C{-}CH{=}CMe(NHCH_2Ph)\}]$ (**5b**). Phenyl, benzyl, and phosphite methyl hydrogen atoms have been omitted. Carbonyl carbons have the same numbers as the oxygen atoms. Ellipsoids are at the 50% probability level.

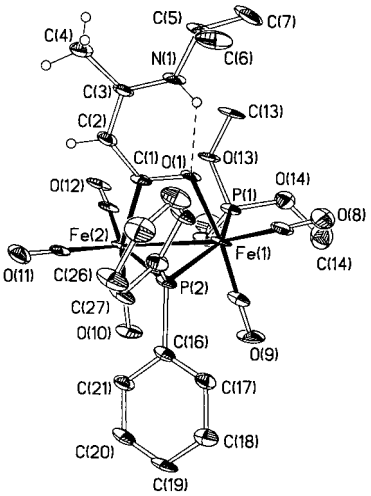

Figure 5. Molecular structure of $[Fe_2(CO)_5\{P(OMe)_3\}(\mu\text{-}PPh_2)\{\mu\text{-}O{=}C{-}CH{=}CMe(NHPr^i)\}]$ (**5a**). Phenyl, isopropyl, and phosphite methyl hydrogen atoms have been omitted. Carbonyl carbons have the same numbers as the oxygen atoms. Ellipsoids are at the 50% probability level.

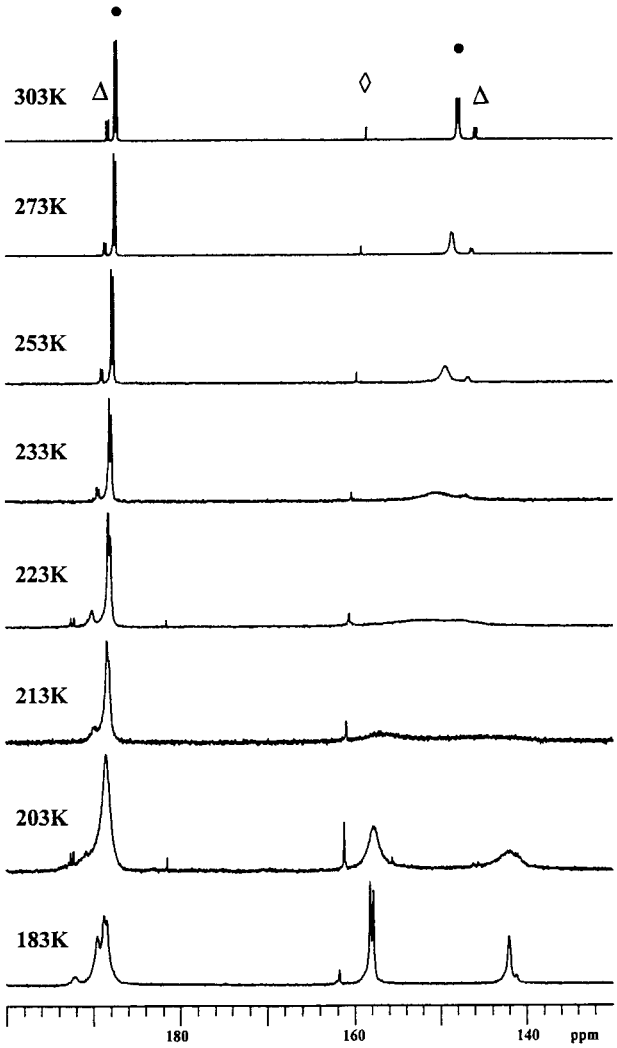

Figure 7. Variable-temperature $^{31}P\{^1H\}$ NMR spectra of $[Fe_2(CO)_5\{P(OMe)_3\}(\mu\text{-}PPh_2)(\mu\text{-}CHC(CH_3)\{NHPr^i\})]$ (**4a**) [●, major endo isomer; △, minor exo isomer; ◇ impurity].

bond correlation study which shows a μ-alkylidene carbon (δ ~78 ppm) in the range expected for an electron-rich M−C−M core and slightly upfield of values previously compiled by Hermann[28] and others.

Full structural details of **4c** have been obtained from a single-crystal X-ray structure determination. A perspective view of the molecular structure together with the atomic-numbering scheme is illustrated in Figure 4 with a selection of bond lengths and angles listed in Table 3. First, we note that **4c** contains a one-atom-bridging alkylidene ligand rather than its β-substituted enamine valence isomer. The two iron atoms are separated by a distance of 2.5656(6) Å and bridged asymmetrically by the alkylidene ligand [Fe(1)−C(1) = 2.019(3) Å, Fe(2)−C(1) = 2.087(3) Å] and a phosphido bridge [Fe(1)−P(2) = 2.2217(8) Å, Fe(2)−P(2) = 2.2345-(9) Å]. The short Fe−Fe bond, together with the concomitant acute FePFe angle [70.30(3)°], results from the presence of the one-atom-bridging hydrocarbyl

(28) (a) Hermann, W. A.; Reiter, B.; Biersack, J. *J. Organomet. Chem*. **1975**, *97*, 245. (b) Hermann, W. A. *Adv. Organomet. Chem*. **1982**, *20*, 159. (c) Hermann, W. A. *Pure Appl. Chem*. **1982**, *54*, 65. (c) Hahn, J. E. *Prog. Inorg. Chem*. **1984**, *31*, 205.

Table 3. Selected Bond Distances (Å) and Angles (deg) for Compound 4c

Fe(1)−Fe(2)	2.5656(6)	Fe(1)−C(1)	2.019(3)
Fe(2)−C(1)	2.087(3)	Fe(1)−P(1)	2.1334(9)
Fe(2)−P(2)	2.2345(9)	Fe(1)−P(2)	2.2217(8)
Fe(1)−C(13)	1.770(3)	Fe(1)−C(14)	1.762(3)
Fe(2)−C(15)	1.801(4)	Fe(2)−C(16)	1.770(3)
Fe(2)−C(17)	1.774(3)	C(1)−C(2)	1.433(4)
C(2)−C(3)	1.503(4)	C(2)−N(1)	1.302(3)
Fe(1)−P(2)−Fe(2)	70.30(3)	P(1)−Fe(1)−P(2)	118.83(3)
P(1)−Fe(1)−C(1)	88.00(8)	C(1)−C(2)−C(3)	119.7(2)
C(1)−C(2)−N(1)	122.0(2)	C(3)−C(2)−N(1)	118.3(3)

ligand.[29] Although short, this distance is significantly longer than the reported value of 2.5477(6) Å in $[Fe_2(CO)_6(\mu\text{-}PPh_2)\{\mu\text{-}CHC(Ph)(NEt_2)\}]$[19d] and is most likely a result of the trans influence of the trimethyl phosphite ligand attached to Fe(1). In comparison, the Fe−Fe bond lengths in the two-atom-bridged complexes $[Fe_2(CO)_6(\mu\text{-}PPh_2)\{\mu\text{-}C(NCyH)C(Ph)H\}]$[19c] and $[Fe_2(CO)_6(\mu\text{-}PPh_2)(\mu\text{-}\eta^1{:}\eta^1\text{-}(Me)C{=}C\{P(OMe)_3\})]$[30] are 2.628(1) and 2.6569(5) Å, respectively, and this elongation is coupled with an increase in the FePFe angle, a reflection of the structural flexibility of the hydrocarbyl-bridged FePFe fragment.[31] Both N(1) and C(2) (sum of angles 360.0°) of the alkylidene ligand are planar, and the C(2)−N(1) bond length [1.302(3) Å] is characteristic of a $C{=}NR_2$ iminium bond, which typically lies in the range 1.287−1.380 Å.[32] This is substantially shorter than the corresponding bond in **3a** [C(2)−N(1) = 1.412(3) Å], the difference (Δ) being 0.110 Å, and comparable to that in **2a** [C(2)−N(1) = 1.325(3) Å]. Surprisingly, the C(1)−C(2) bond length [1.433(4) Å] is shorter than that expected based on reported values of $C(sp^2)-C(sp^3)$ single bonds [1.51 Å], which reflects some delocalization over the bridging hydrocarbyl fragment despite the tetrahedral nature of C(1). The dihedral angle of 37° between the plane containing N(1), C(2), C(3) and H(1A), C(1), C(2) is slightly larger than previously reported values, and the small angle subtended by the metal atoms at the μ-CHR bridge [77.32(9)°] is characteristic of binuclear alkylidene complexes. One of the iron atoms, Fe(2), supports three terminal carbonyl ligands, one trans to the phosphido bridge, one trans to the Fe−Fe bond, and the remaining one cis, while Fe(1) supports two carbonyl ligands and one trimethyl phosphite, the latter trans to the Fe−Fe bond.

In the absence of the stabilizing Fe−N interaction in **3**, the bridging hydrocarbyl fragment isomerizes to its alkylidene valence form, manifested in the short C(2)−N(1) bond and long Fe(2)−C(2) nonbonding distance. The unexpected stability of **3** with respect to its alkylidene valence isomer most likely arises from coordination of the β-amino substituent to Fe(1), which prevents the nitrogen lone pair from participating in N(pπ)−C(pπ) overlap. In contrast, the recently prepared β-phosphino-substituted complex $[Fe_2(CO)_6(\mu\text{-}PPh_2)\{\mu\text{-}\eta^1{:}\eta^2\text{-}MeC{=}CH(PPh_2)\}]$[10a] prefers to exist as its $\mu\text{-}\mu^1{:}\eta^2$-alkenyl coordination isomer, leaving a stereochemically active lone pair of electrons on the phosphorus atom. These ideas suggest that the structure of σ−η-alkenyl complexes depends largely on the nature of the β-substituent, a factor which is also thought to influence the free energy of activation for σ−η-windshield-wiper exchange.

Transformation of 2a into the α,β-Unsaturated Bridging Acyl Complexes $[Fe_2(CO)_5\{P(OMe)_3\}(\mu\text{-}PPh_2)\{\mu\text{-}O{=}C{-}CH{=}CMe(NHR)\}]$ (5a). While solutions of **3a** react with trimethyl phosphite to give **4a**, treatment of a refluxing toluene solution of **2a** with trimethyl phosphite gave the α,β-unsaturated acyl complex $[Fe_2(CO)_5\{P(OMe)_3\}(\mu\text{-}PPh_2)\{\mu\text{-}O{=}C{-}CH{=}CMe(NPr^iH)\}]$ (**5a**). This reaction is conveniently monitored using TLC and IR spectroscopy, with the appearance of a new $\nu(C{=}O)$ band at 1560 cm^{-1} typical of a carbonyl absorption of a bridging acyl ligand.[33] The most striking feature of the $^{31}P\{^1H\}$ NMR spectrum of **5a** is the presence of a line-broadened high-field resonance, while the low-field signal appears as a sharp doublet. We have already noted similar line-broadening features in the $^{31}P\{^1H\}$ NMR spectrum of **4a**, the details of which will be described in the following section (vide infra). One of these resonances is characteristic of a phosphido ligand bridging a metal−metal bond and the other a metal-bound trimethyl phosphite ligand. In the $^{13}C\{^1H\}$ NMR spectrum, the acyl carbon appears in the low-field region at δ 255.6, typical of a μ-acyl-bridged complex.[34]

Full structural details of the bridging acyl ligand and the position of substitution were provided by single-crystal X-ray analyses of **5a** and **5b**. Since these structures differ in the position of phosphite substitution, both will be discussed in detail. Perspective views of the molecular structures of **5a** and **5b**, together with the atomic-numbering schemes, are illustrated in Figures 5 and 6, respectively, and a selection of bond distances and angles for both compounds listed in Table 4. The two iron atoms in **5b** are separated by a distance of 2.6121(6) Å and bridged asymmetrically by a phosphido ligand [Fe(1)−P(2) = 2.2214(8) Å, Fe(2)−P(2) = 2.2138(9) Å] and an acyl ligand, oxygen-bound to Fe(1) [Fe(1)−O(1) = 1.9899(18) Å] and carbon-bound to Fe(2) [Fe(2)−C(1) = 1.982(3) Å]. The corresponding bond lengths for **5a** are similar though less precise (Table 4). The acyl C(1)−O(1) bond length in **5a** [1.284 (7) Å] and **5b** [1.288(3) Å] is similar to previously reported values and longer than a typical conjugated C−O double bond. Although described as an α,β-unsaturated acyl ligand, the C(1)−C(2) bond length in **5a** [1.415(8) Å] and **5b** [1.415(4) Å] is significantly shorter than expected for a carbon−carbon single bond adjacent to a carbonyl fragment [1.516(5) Å].[35] In addition, the C(2)−C(3) bond of 1.401(8) Å (**5a**) [1.387(4) Å, (**5b**)] shows a substantial elongation from that of a typical carbon−carbon double

(29) Cherkas, A. A.; Hoffman, D.; Taylor, N. J.; Carty, A. J. *Organometallics* **1987**, *6*, 1466.
(30) Doherty, S.; Elsegood, M. R. J.; Clegg, W.; Ward, M.; Waugh, M. *Organometallics* **1997**, *16*, 4251.
(31) Carty, A. J.; MacLaughlin, S. A.; Nicciarone, D. *In Phosphorus-31 NMR Spectroscopy in Stereochemical Analysis: Organic Compounds and Metal Complexes*; Verkade, J. G., Quinn, L. D., Eds.; VCH: New York, 1987, Chapter 16, pp 54−619. (b) Carty, A. J. *Adv. Chem Ser.* **1982**, *196*, 163.
(32) Merenyi, R. *Adv. Org. Chem.* **1976**, *9*, 90.
(33) (a) Seyferth, D.; Archer, C. M.; Ruschke, D. P.; Cowie, M.; Hilts, R. W. *Organometallics* **1991**, *10*, 3363. (b) Seyferth, D.; Womack, C. B.; Dewan, J. C. *Organometallics* **1985**, *4*, 398. (c) Hogarth, G.; Lavender, M. H.; Shukri, K. *J. Organomet. Chem.* **1997**, *527*, 247.
(34) (a) Yu, Y.-F.; Gallucci, J.; Wojcicki, A. *J. Am. Chem. Soc.* **1983**, *105*, 4826. (b) Seyferth, D.; Hoke, J. B.; Dewan, J. C.; Hofmann, P.; Schnellbach, H. *Organometallics* **1994**, *13*, 3452. (c) Rosen, R. P.; Hoke, J. B.; Whittle, R. R.; Geoffroy, G. L.; Hutchinson, J. P.; Zubieta, J. A. *Organometallics* **1984**, *3*, 836.
(35) *International Tables for X-ray Crystallography*; MacGillavry, C. M., Rieck, G. D., Eds.; Kynoch Press: Birmingham, England, 1974; Vol. 3, p 276.

Table 4. Selected Bond Distances (Å) and Angles (deg) for Compounds 5a and 5b

compd **5a**		compd **5b**	
Fe(1)−Fe(2)	2.6177(13)	Fe(1)−Fe(2)	2.6121(6)
F(1)−P(2)	2.229(19)	Fe(1)−P(2)	2.2214(8)
Fe(2)−P(2)	2.2148(18)	Fe(2)−P(2)	2.2138(9)
Fe(1)−O(1)	1.996(4)	Fe(1)−O(1)	1.9899(18)
Fe(2)−C(1)	1.977(6)	Fe(2)−C(1)	1.982(3)
Fe(1)−P(1)	2.1895(19)	Fe(1)−P(1)	2.1725(10)
Fe(1)−C(8)	1.784(7)	Fe(1)−C(12)	1.797(3)
Fe(1)−C(9)	1.744(6)	Fe(1)−C(13)	1.746(3)
Fe(2)−C(10)	1.804(6)	Fe(2)−C(14)	1.781(3)
Fe(2)−C(11)	1.779(7)	Fe(2)−C(15)	1.811(3)
Fe(2)−C(12)	1.803(6)	Fe(2)−C(16)	1.787(3)
C(1)−O(1)	1.284(7)	C(1)−O(1)	1.288(3)
C(1)−C(2)	1.415(8)	C(1)−C(2)	1.415(4)
C(2)−C(3)	1.401(8)	C(2)−C(3)	1.387(4)
C(3)−N(1)	1.317(8)	C(3)−N(1)	1.319(4)
Fe(1)−P(2)−Fe(2)	72.30(6)	Fe(1)−P(2)−Fe(2)	72.16(3)
P(1)−Fe(1)−C(8)	103.1(2)	P(1)−Fe(1)−C(12)	102.95(11)
P(1)−Fe(1)−C(9)	88.9(2)	P(1)−Fe(1)−C(13)	93.45(11)
O(1)−C(1)−C(2)	121.2(5)	O(1)−C(1)−C(2)	118.8(3)
C(1)−C(2)−C(3)	124.5(6)	C(1)−C(2)−C(3)	125.1(3)
C(2)−C(3)−N(1)	121.6(6)	C(2)−C(3)−N(1)	122.4(1)
C(2)−C(3)−C(4)	118.8(6)	C(2)−C(3)−C(4)	119.2(3)
N(1)−C(3)−C(4)	119.6(5)	N(1)−C(3)−C(4)	118.4(3)
C(3)−N(1)−C(5)	128.1(5)	C(3)−N(1)−C(5)	128.1(2)

bond [1.337(6) Å]. Moreover, the C(3)−N(1) distance of 1.317(8) Å (**5a**) [1.319(4) Å, (**5b**)] is characteristic of a C−N bond in an iminium salt, which typically lies between 1.287 and 1.38 Å. These bond lengths suggest significant delocalization within the amino-substituted α,β-unsaturated acyl ligand, which is further reinforced by the approximate planarity of the O(1), C(1), C(2), C(3), N(1) unit. While the core structural features of **5a** and **5b**, in particular the bond lengths and angles within the bridging hydrocarbyl ligand, the metal−metal, metal phosphido, and metal acyl bridge are essentially the same, they differ in the site of phosphite substitution. In **5a**, the phosphite is located on the iron atom σ-bonded to the acyl oxygen, Fe(1), and trans to the phosphido bridge, while in **5b**, the phosphite is located on the same iron atom but trans to the Fe−Fe bond. The low-temperature ^{31}P NMR spectrum of **5a** (vide infra) contains two sets of resonances in a 4:1 ratio, which we suggest belong to isomers that differ in the position of substitution of the trimethyl phosphite ligand, either trans to the Fe−Fe bond or trans to the μ-PPh_2 group. The imine hydrogen is involved in intramolecular hydrogen bonding to the oxygen atom of the bridging acyl ligand (N- - -O distance = 2.662 Å in **5a** and 2.637 Å in **5b**; N(1)−H(1)-O(1) angle 135° in **5a** and **5b**) to form a planar six-membered ring containing O(1), C(1), C(2), C(3), N(1), and H(1) (rms deviation from mean plane 0.042 Å in **5a** and 0.02 Å in **5b**).

Carty and co-workers have previously prepared[36] similar α,β-unsaturated acyl complexes via carbonylative-amination of the multisite bound acetylide [$Fe_2(CO)_6$(μ-PPh_2)(μ-C≡CR)]. Several mechanisms were discussed, the most favored of which was suggested to be direct CO insertion into a dipolar μ-alkylidene intermediate, itself formed via addition of amine to C_β of the acetylide. Minute amounts of this acyl complex have previously been isolated from the reaction between aniline and the parent acetylide, which gave the μ-alkylidene complex [$Fe_2(CO)_6$(μ-PPh_2){μ-CHCPh(NHPh)}] as the dominant product. Our attempts to carbonylate **4a** in refluxing toluene led to the isolation of **5a** (Scheme 1) together with low yields of several unidentified products. Supporting these observations, we noted the appearance of a number of additional products during our high-temperature ^{31}P NMR studies with **4a**, none of which corresponded to **5a**. This suggests that **4a** is unstable and that its carbonylation in refluxing toluene must compete with other transformations. Complexes **5a** and **5b** are stable with respect to loss of carbon monoxide, even after 24 h at reflux in toluene. In contrast, Seyferth and co-workers have reported that diiron thiolate-bridged α,β-unsaturated acyl complexes are unstable toward decarbonylation and lose CO even at room temperature. Although we cannot yet provide a definitive explanation for the enhanced stability of **5a** and related α,β-unsaturated complexes, with respect to decarbonylation, it is worth noting that the carbon−carbon bond to the acyl carbon in **5a** [1.415(8) Å] and **5b** [1.415(4) Å] is substantially shorter than that in [$Fe_2(CO)_6$(μ-SBut){μ-O=C−C(OEt)=CH_2}] [1.504(4) Å],[34b] which suggests that there is extensive electron delocalization in the former while the latter contains localized double and single bonds.

Variable-Temperature ^{31}P{^{1}H} NMR Studies. The room temperature ^{31}P{^{1}H} NMR spectra of [$Fe_2(CO)_5${P(OMe)$_3$}(μ-PPh_2){μ-C(H)CMe(NHPr^i)}] (**4a**) and [$Fe_2(CO)_5${P(OMe)$_3$}(μ-PPh_2){μ-O=C−CH=CMe(NHCH$_2$Ph)}] (**5b**) contain two signals, a sharp low-field doublet associated with the metal-coordinated trimethyl phosphite ($^2J_{PP}$ = 44.5 Hz, **4a**; 62.0 Hz, **5b**) and an exchange-broadened high-field doublet which belongs to the bridging phosphido ligand. To investigate this exchange process further, variable-temperature ^{31}P{^{1}H} NMR studies were performed with **4a** and **5b**, the results of which are shown in Figures 7 and 8, respectively. Qualitatively both compounds exhibit similar line-broadening characteristics within the temperature range 185−255 K. Low-temperature ^{31}P{^{1}H} NMR studies show that at −85 °C **4a** exists as a 2:1 mixture of two distinct isomers in slow exchange and that each isomer comprises one trimethyl phosphite and one phosphido bridge. In the case of **4a**, the trimethyl phosphite resonances associated with the major and minor isomers appear as separate well-resolved signals at δ 158.2 and 142.2 while the resonances belonging to the phosphido bridge are only poorly resolved and appear as a broad doublet at δ 189.0 ($^2J_{PP}$ = 73.0 Hz) overlapping a broad singlet at δ 189.8 ($^2J_{PP}$ = 37.0 Hz, calculated from the averaged value of $^2J_{PP}$ observed at high temperature), the latter of which corresponds to the minor component. The temperature dependence of the ^{31}P{^{1}H} spectra clearly shows that these two isomers interconvert. As the temperature is raised, both sets of resonances broaden, first those at low-field while the high-field signals only start to coalesce at much higher temperatures. Above room temperature, the major and minor isomers interconvert rapidly to give an averaged ^{31}P NMR spectrum that contains a pair of high- and low-

(36) Mott, G. N.; Granby, R.; MacLaughlin, S. A.; Taylor, N. J.; Carty, A. J. *Organometallics* **1982**, *1*, 189.

(37) (a) Cooke, J.; Takats, J. *Organometallics* **1995**, *14*, 698. (b) Alex, R. F.; Pomeroy, R. K. *Organometallics* **1987**, *6*, 2437. (c) Cooke, J.; McClung, R. E. D.; Takats, J.; Rogers, R. D. *Organometallics* **1996**, *15*, 4459. (d) Deeming, A. J. *Adv. Organomet. Chem*. **1986**, *26*, 1. (e) Heyes, S. J.; Gallop, M. A.; Johnson, B. F. G.; Lewis, J.; Dobson, C. M. *Inorg. Chem*. **1991**, *30*, 3850.

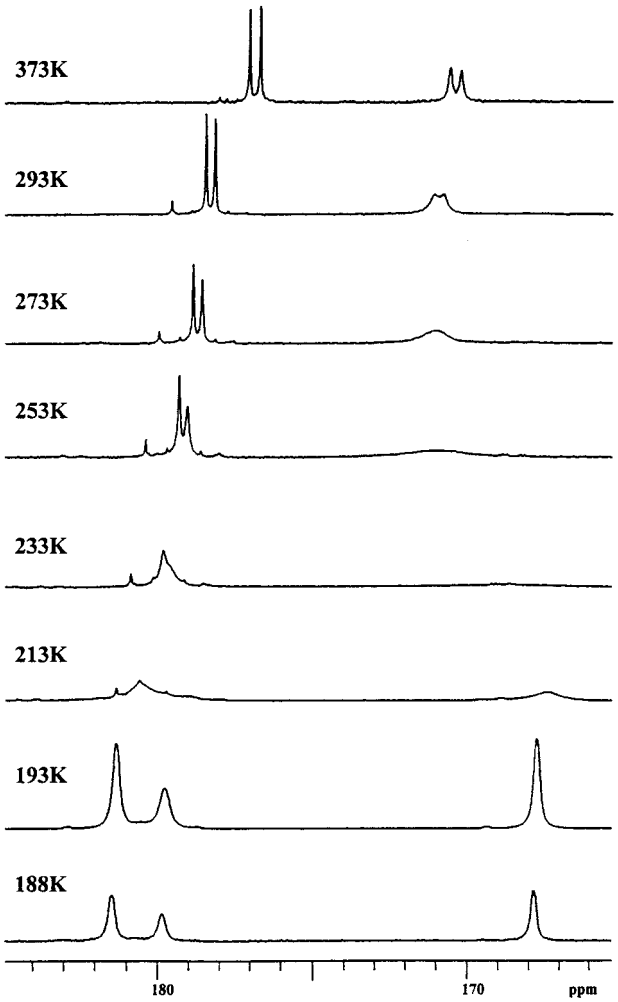

Figure 8. Variable-temperature $^{31}P\{^1H\}$ NMR spectra $[Fe_2(CO)_5\{P(OMe)_3\}(\mu\text{-}PPh_2)\{\mu\text{-}O{=}C{-}CH{=}CMe(NHCH_2\text{-}Ph)\}]$ (**5b**).

field doublets. Since these changes are reversible and the $^2J_{PP}$ coupling is maintained at high temperatures, the isomer interconversion must be intramolecular.

Similar behavior was observed for **5b**, although the low-temperature $^{31}P\{^1H\}$ NMR spectrum only contains three resonances, two of which are well-separated and belong to the major isomer (δ 181.4 and 167.8 ppm) while the signals associated with the trimethyl phosphite and bridging phosphido ligands of the minor component are coincident at δ 180.0, an assignment which has been confirmed using low-temperature 2D $^{31}P{-}^{31}P$ exchange experiments.

The close similarity between the variable-temperature $^{31}P\{^1H\}$ NMR spectra of **4a** and **5b** suggests that a similar dynamic process is responsible for the line broadening associated with both compounds. The spectroscopic characteristics and the free energy of activation for this exchange ($\Delta G^{\ddagger}_{273}$ = 9.5 kcal mol^{-1}, **4a**; $\Delta G^{\ddagger}_{273}$ = 10.4 kcal mol^{-1}, **5b**), determined from a lineshape analysis of the spectra in Figures 7 and 8, are consistent with the dynamic process shown in Scheme 9, which involves interchange of two isomers via a restricted trigonal twist at the phosphite-substituted iron center. This mechanism interchanges the major isomer, with the trimethyl phosphite trans to the phosphido bridge ($^2J_{PP}$ = 73.0 Hz), with the minor isomer, in which the phosphite occupies the site trans

Scheme 9

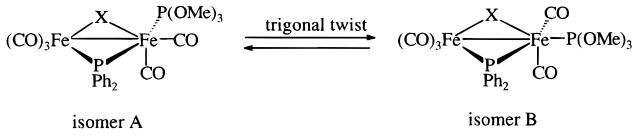

isomer A isomer B

to the iron−iron bond ($^2J_{PP}$ = 37.0 Hz). These conclusions are further reinforced by the solid-state structures of **5a** and **5b**, which correspond to the two proposed substitutional isomers, albeit with different acyl substituents (vide supra). The free energy of activation associated with the trigonal twist mechanism in **4a** and **5b** are lower than the previously reported values of $\Delta G^{\ddagger}$ = 15.1 kcal mol^{-1} for $[Os_2Rh(CO)_8(\eta^5\text{-}C_5H_5)PMe_3]$,[15a] $\Delta G^{\ddagger}$ = 15.0 kcal mol^{-1} for $[Os_3(CO)_{10}\{P(OMe)_3\}_2]$,[15b] and $\Delta G^{\ddagger}$ = 13.8 kcal mol^{-1} for $[Os_3(CO)_9\{P(OMe)_3\}_3]$.[15b] The trigonal twist that interconverts the isomers of each of these three complexes occurs at an osmium center, for which a greater free energy of activation is expected. Surprisingly, the free energy of activation for the interconversion of isomers of $[Os_2Pt(CO)_8(PPh_3)_2]$ ($\Delta G^{\ddagger}$ = 11.8 kcal mol^{-1}),[15c] again via a trigonal twist mechanism,[15d,e] is unusually low and much closer to those reported here.

Conclusions

The dimetallacyclopentane derivatives $[Fe_2(CO)_6(\mu\text{-}PPh_2)\{\mu{-}\eta^1{:}\eta^1\text{-}H_2C{-}C(NHR){-}CH_2\}]$ (R = Pr^i (**2a**), CH_2-Ph (**2b**), C_6H_{11} (**2c**), Pr^n (**2d**)) are conveniently prepared via the addition of primary amines to C_β of the allenyl ligand in $[Fe_2(CO)_6(\mu\text{-}PPh_2)\{\mu{-}\eta^1{:}\eta^2\text{-}(H)C{=}C{=}CH_2\}]$ (**1**). Although stable in the crystalline state, in solution **2a**−**d** readily rearrange to give the nitrogen-coordinated enamines $[Fe_2(CO)_5(\mu\text{-}PPh_2)\{\mu{-}\eta^1(C){:}\eta^2(C){:}\eta^1(N)\text{-}(H)C{=}CCH_3(NHR)\}]$ (R = Pr^i (**3a**), CH_2Ph (**3b**), C_6H_{11} (**3c**), Pr^n (**3d**)) via loss of CO and a 1,3-hydrogen migration. While α- and β-substituted enamines have been proposed as intermediates in the addition of primary and secondary amines to $[Fe_2(CO)_6(\mu\text{-}PPh_2)\{\mu{-}\eta^1{:}\eta^2\text{-}C{\equiv}CR\}]$, **3a**−**d** are the first such complexes to be isolated and spectroscopically and crystallographically characterized. In addition, the $\sigma{-}\eta$-alkenyl ligand in $[Fe_2(CO)_5(\mu\text{-}PPh_2)\{\mu{-}\eta^1(C){:}\eta^2(C){:}\eta^1(N)\text{-}(H)C{=}CCH_3(NHPr^i)\}]$ (**3a**) adopts a highly unusual exo conformation with respect to the phosphido bridge. As expected, **3a** and **3c** react with trimethyl phosphite to afford the alkylidene-bridged complexes $[Fe_2(CO)_5\{P(OMe)_3\}(\mu\text{-}PPh_2)\{\mu\text{-}CHCMe(NHR)\}]$ (R = Pr^i (**4a**), C_6H_{11} (**4c**)). Prolonged thermolysis of a toluene solution of **4a** in the presence of CO affords the α,β-unsaturated acyl complexes $[Fe_2(CO)_5\{P(OMe)_3\}(\mu\text{-}PPh_2)\{\mu\text{-}O{=}C{-}CH{=}CMe(NHPr^i)\}]$ (**5a**), albeit in low yields. Improved yields of **5a** were obtained by heating toluene solutions of **2a** in the presence of excess trimethyl phosphite, during which there was no evidence for the formation of **4a**, which suggests that these two products are most likely formed via different pathways. Overall, the products derived from the rearrangement of **2a**−**d** closely resembles those of nucleophilic addition to the parent acetylide $[Fe_2(CO)_6(\mu\text{-}PPh_2)\{\mu{-}\eta^1{:}\eta^2\text{-}C{\equiv}CCH_3\}]$, a tautomer of the allenyl complex. We are currently exploring the scope of these transformations by using functionalized amines to prepare more elaborate α,β-

unsaturated amines. In solution, compounds **4** and **5** exists as a mixture of two interconverting isomers, and variable-temperature ^{31}P NMR studies were used to examine the mechanism and determine the activation parameters for this interconversion. The line-broadening characteristics and the free energy of activation are consistent with a mechanism that involves a restricted trigonal twist at the phosphite-substituted iron center.

Experimental Section

General Procedures. Unless otherwise stated, all manipulations were carried out in an inert atmosphere glovebox or by using standard Schlenk-line techniques. Diethyl ether and hexane were distilled from Na/K alloy, tetrahydrofuran from potassium, and dichloromethane from CaH_2. $CDCl_3$ was predried with CaH_2 and vacuum transferred and stored over 4 Å molecular sieves. Infrared spectra were recorded on a Mattson Genesis FTIR spectrometer operating WINFIRST software. Reactions were monitored by thin-layer chromatography (Baker flex silica gel, 1B-F).Variable-temperature ^{31}P NMR spectra were recorded on a JEOL LAMBDA 500, and 2D ^{31}P−^{31}P exchange spectra were run at −80 °C. Column chromatography was carried out with alumina purchased from Aldrich Chemical Co. and deactivated with 6% w/w water prior to loading. Trimethyl phosphite was purchased from Strem Chemical Co. and used without further purification. The diiron complex $[Fe_2(CO)_6(\mu\text{-PPh}_2)\{\mu-\eta^1:\eta^2\text{-C(H)=C=CH}_2\}]$ was prepared as previously described.[10a]

Preparation of $[Fe_2(CO)_6(\mu\text{-PPh}_2)(\mu-\eta^1:\eta^1\text{-}\{H_2C-C(NHPr^i)-CH_2\})]$ (2a). An excess of isopropylamine (0.4 mL, 9.8 mmol) was added to a solution of $[Fe_2(CO)_6(\mu\text{-PPh}_2)\{\mu-\eta^1:\eta^2\text{-C(H)=C=CH}_2\}]$ (0.200 g, 0.4 mmol) in diethyl ether (20 mL). The reaction mixture was allowed to stir overnight, during which time the color changed from pale yellow to orange. The solvent was removed under reduced pressure to leave an oily residue. This residue was dissolved in the minimum volume of dichloromethane (1−2 mL) desolvated, placed on a 330 × 30 mm column, and eluted with dichloromethane/*n*-hexane (30/70, v/v). The first major yellow band to elute was collected and crystallized from *n*-hexane to give **2a** as yellow crystals in 65% yield (0.14 g). IR (ν(CO), cm^{-1}, C_6H_{14}): 2045 m, 2004 s, 1976 s, 1958 s, 1940 w. ^{31}P{^{1}H} NMR (202.35 MHz, $CDCl_3$, 298 K, δ): 191.6 (s, μ-PPh$_2$). ^{1}H NMR (200.1 MHz, $CDCl_3$, 298 K, δ): 7.83−7.68 (m, 4H, C_6H_5), 7.39−7.14 (m, 6H, C_6H_5), 5.13 (br d, $^3J_{HH}$ = 8.4 Hz, 1H, N−*H*), 3.62 (sept, $^3J_{HH}$ = 6.7 Hz, 1H, C*H*−(CH$_3$)$_2$), 1.24 (d, $^3J_{HH}$ = 6.7 Hz, 3H, CH(C*H*$_3$)$_2$), 1.15 (t, $^2J_{HH} = {}^3J_{PH}$ = 8.2 Hz, 1H, C$_\gamma$*H*), 1.0 (d, $^3J_{HH}$ = 6.7 Hz, 3H, CH(C*H*$_3$)$_2$), 1.0 (s, 1H, C$_\alpha$*H*), 0.97 (m, 1H, C$_\alpha$*H*), 0.74 (m, 1H, C$_\gamma$*H*). ^{13}C{^{1}H} NMR (125.65 MHz, $CDCl_3$, 298 K, δ): 217.3 (d, $^2J_{PC}$ = 32.7 Hz, CO), 215.8 (m, CO), 211.4 (d, $^2J_{PC}$ = 17.6 Hz, CO), 208.4 (d, $^2J_{PC}$ = 11.6 Hz, CO), 191.8 (s, C$_\beta$), 142.4 (d, $^1J_{PC}$ = 36.5 Hz, *C*$_6$H$_5$), 139.4 (d, $^1J_{PC}$ = 20.1 Hz, *C*$_6$H$_5$), 133.7 (d, $^2J_{PC}$ = 6.3 Hz, *C*$_6$H$_5$), 132.3 (d, $^2J_{PC}$ = 8.8 Hz, *C*$_6$H$_5$), 129.1−128.1 (m, *C*$_6$H$_5$), 45.7 (s, N−*C*H(CH$_3$)$_2$), 23.3 (s, CH(*C*H$_3$)$_2$), 22.4 (s, CH(*C*H$_3$)$_2$), 15.0 (d, $^2J_{PC}$ = 7.9 Hz, C$_\gamma$), 7.6 (d, $^2J_{PC}$ = 7.6 Hz, C$_\alpha$). Anal. Calcd for $C_{24}H_{22}Fe_2NO_6P$: C, 51.19; H, 3.94; N, 2.49. Found: C, 51.13; H, 3.86; N, 2.46.

Compounds **2b**−**d** were prepared using a procedure similar to that described for **2a**. Selected spectroscopic and analytical data are listed for each compound.

Preparation of $[Fe_2(CO)_6(\mu\text{-PPh}_2)(\mu-\eta^1:\eta^1\text{-}\{H_2C-C(NHCH_2Ph)-CH_2\})]$ (2b). Obtained as yellow crystals in 72% yield from *n*-hexane at room temperature. IR (ν(CO), cm^{-1}, C_6H_{14}): 2046 m, 2005 s, 1977 s, 1959 s, 1941 w. ^{31}P{^{1}H} NMR (202.35 MHz, $CDCl_3$, 298 K, δ): 191.3 (s, μ-PPh$_2$). ^{1}H NMR (500.1 MHz, $CDCl_3$, 298 K, δ): 7.83−7.69 (m, 4H, C_6H_5), 7.32−7.12 (m, 11H, C_6H_5), 5.49 (br m, 1H, N−*H*), 4.45 (br m, 1H, C*H*$_a$H$_b$Ph), 4.35 (br m, 1H, CH$_a$*H*$_b$Ph), 1.31 (br m, 1H, C$_\gamma$H), 1.24 (br m, 1H, C$_\alpha$*H*), 1.00 (br m, 1H, C$_\alpha$*H*), 0.86 (br m, 1H, C$_\gamma$*H*). ^{13}C{^{1}H} NMR (125.65 MHz, $CDCl_3$, 298 K, δ): 217.5 (d, $^2J_{PC}$ = 32.0 Hz, CO), 206.9 (d, $^2J_{PC}$ = 32.7 Hz, CO), 191.4 (s, C$_\beta$), 142.2 (d, $^1J_{PC}$ = 36.5 Hz, *C*$_6$H$_5$), 139.2 (d, $^1J_{PC}$ = 20.1 Hz, *C*$_6$H$_5$), 133.7 (d, $^2J_{PC}$ = 7.6 Hz, *C*$_6$H$_5$), 133.2 (d, $^2J_{PC}$ = 7.6 Hz, *C*$_6$H$_5$), 129.5−128.0 (m, *C*$_6$H$_5$), 48.2 (s, N−*C*H$_2$), 14.6 (br s, C$_\gamma$), 7.6 (br s, C$_\alpha$). Anal. Calcd for $C_{28}H_{22}Fe_2NO_6P$: C, 54.99; H, 3.63; N, 2.30. Found: C, 54.68; H, 3.86; N, 2.43.

Preparation of $[Fe_2(CO)_6(\mu\text{-PPh}_2)(\mu-\eta^1:\eta^1\text{-}\{H_2C-C(NHC_6H_{11})-CH_2\})]$ (2c). Obtained as yellow crystals in 68% yield from *n*-hexane at room temperature. IR (ν(CO), cm^{-1}, C_6H_{14}): 2044 m, 2004 s, 1974 s, 1957 s, 1949 w. ^{31}P{^{1}H} NMR (202.35 MHz, $CDCl_3$, 298 K, δ): 191.8 (s, μ-PPh$_2$). ^{1}H NMR (200.1 MHz, $CDCl_3$, 298 K, δ): 7.90−7.10 (m, 10H, C_6H_5), 5.20 (br d, $^3J_{HH}$ = 8.2 Hz, 1H, N−*H*), 3.21 (m, N−C−*H*, 1H), 1.93 (s, 4H, Fe−C*H*$_2$), 1.7−0.7 (m, 10H, Cy−C*H*$_2$). ^{13}C{^{1}H} NMR (125.65 MHz, $CDCl_3$, 298 K, δ): 205 (br s, CO), 191.6 (s, C$_\beta$), 133.0−128.1 (m, *C*$_6$H$_5$), 52.6 (s, Cy−*C*−N), 33.8 (s, Cy−CH$_2$), 32.8 (s, Cy−CH′$_2$), 25.2 (s, Cy−C″H$_2$), 24.6 (d, $^2J_{PC}$ = 4.0 Hz, *C*$_\gamma$H$_2$), 7.6 (s, $^2J_{PC}$ = 7.6 Hz, *C*$_\alpha$H$_2$). Anal. Calcd for $C_{27}H_{26}Fe_2NO_6P\cdot C_2H_3N$: C, 54.01; H, 4.54; N, 4.35. Found: C, 53.60; H, 4.32; N, 4.21.

Preparation of $[Fe_2(CO)_6(\mu\text{-PPh}_2)(\mu-\eta^1:\eta^1\text{-}\{H_2C-C(NHCH_2CH_2CH_3)-CH_2\})]$ (2d). Obtained as yellow-orange crystals in 70% yield from *n*-hexane at room temperature. IR (ν(CO), cm^{-1}, C_6H_{14}): 2046 m, 2006 s, 1977 s, 1957 s, 1941 w. ^{31}P{^{1}H} NMR (202.35 MHz, $CDCl_3$, 298 K, δ): 192.6 (s, μ-PPh$_2$). ^{1}H NMR (200.1 MHz, $CDCl_3$, 298 K, δ): 7.79−7.12 (m, 10H, C_6H_5), 5.17 (br m, 1H, N−*H*), 3.14 (m, 1H, N−C*H*$_a$H$_b$-CH$_2$CH$_3$), 3.08 (m, 1H, N−CH$_a$*H*$_b$CH$_2$CH$_3$), 1.46 (m, 2H, N−CH$_2$C*H*$_2$CH$_3$), 1.19 (t, $^2J_{HH} = {}^3J_{PH}$ = 8.3 Hz, 1H, C$_\gamma$*H*), 1.03 (s, 1H, C$_\alpha$*H*), 0.85 (t, $^3J_{HH}$ = 7.4 Hz, 3H, N−CH$_2$CH$_2$C*H*$_3$), 0.81 (br m, 1H, C$_\alpha$*H*), 0.71 (br m, 1H, C$_\gamma$*H*). ^{13}C{^{1}H} NMR (125.65 MHz, $CDCl_3$, 298 K, δ): 217.2 (d, $^2J_{PC}$ = 32.7 Hz, CO), 215.9 (m, CO), 214.4 (s, CO), 211.4 (d, $^2J_{PC}$ = 17.6 Hz, CO), 192.1 (s, C$_\beta$), 142.4 (d, $^1J_{PC}$ = 36.2 Hz, *C*$_6$H$_5$), 139.5 (d, $^2J_{PC}$ = 19.6 Hz, *C*$_6$H$_5$), 135.8−127.6 (m, *C*$_6$H$_5$), 45.8 (s, N−CH$_2$CH$_2$CH$_3$), 22.7 (s, N−CH$_2$CH$_2$CH$_3$), 14.9 (s, C$_\gamma$), 11.3 (s, N−CH$_2$CH$_2$CH$_3$), 7.5 (s, C$_\alpha$). Anal. Calcd for $C_{24}H_{22}Fe_2NO_6P$: C, 51.19; H, 3.94; N, 2.49. Found: C, 50.97; H, 3.77; N, 2.43.

Preparation of $[Fe_2(CO)_5(\mu\text{-PPh}_2)(\mu-\eta^1(C):\eta^2(C):\eta^1(N)\text{-}\{HC=C(NHPr^i)CH_3\})]$ (3a). Complex **2a** (0.08 g, 0.14 mmol) was dissolved in 30 mL of toluene, and the solution was heated at reflux for 2 h, during which time the reaction mixture turned from yellow to deep red. The solvent was removed to leave a red oily residue, which was dissolved in dichloromethane, absorbed onto deactivated alumina placed on a 30 × 300 mm column, and eluted with dichloromethane−*n*-hexane (20/80, v/v). A single major red band eluted, which was collected and crystallized from dichloromethane−*n*-hexane to yield deep red crystals of **3a** in 68% yield (0.05 g). IR (ν-(CO), cm^{-1}, C_6H_{14}): 2027 m, 1981 s, 1959 s, 1928 m. ^{31}P{^{1}H} NMR (202.35 MHz, $CDCl_3$, 298 K, δ): 152.2 (s, μ-PPh$_2$). ^{1}H NMR (500.1 MHz, $CDCl_3$, 298 K, δ): 7.51−7.48 (m, 4H, C_6H_5), 7.21−7.17 (m, 6H, C_6H_5), 4.72 (d, $^3J_{PH}$, 20.5 Hz, 1H, *H*C=CCH$_3$), 3.44 (d, $^3J_{PH}$ = 9.5 Hz, 1H, N−*H*), 3.11 (m, 1H, C*H*(CH$_3$)$_2$), 2.29 (s, 3H, C=CC*H*$_3$), 1.49 (d, $^3J_{HH}$ = 6.4 Hz, 3H, CH(C*H*$_3$)$_2$), 1.33 (d, $^3J_{HH}$ = 6.6 Hz, 3H, CH(C*H*$_3$)$_2$). ^{13}C{^{1}H} NMR (125.65 MHz, $CDCl_3$, 298 K, δ): 220.7 (d, $^2J_{PC}$ = 17.6 Hz, CO), 214.5 (d, $^2J_{PC}$ = 3.1 Hz, CO), 210.1 (d, $^2J_{PC}$ = 11.4 Hz, CO), 140.4 (d, $^1J_{PC}$ = 28.0 Hz, *C*$_6$H$_5$), 139.2 (d, $^1J_{PC}$ = 34.1 Hz, *C*$_6$H$_5$), 133.1 (d, $^2J_{PC}$ = 8.3 Hz, *C*$_6$H$_5$), 132.6 (d, $^2J_{PC}$ = 9.3 Hz, *C*$_6$H$_5$), 129.3−127.8 (m, *C*$_6$H$_5$), 126.7 (d, $^2J_{PC}$ = 40.3 Hz, H*C*=CCH$_3$), 120.1 (s, C=*C*CH$_3$), 51.7 (s, *C*H(CH$_3$)$_2$), 25.4 (s, CH(*C*H$_3$)$_2$), 23.9 (s, CH(*C*H$_3$)$_2$), 23.3 (s, C=C*C*H$_3$). Anal. Calcd for $C_{23}H_{22}Fe_2NO_5P$: C, 51.63; H, 4.14; N, 2.62. Found: C, 51.74; H, 4.14; N, 2.60.

Compounds **3b**−**d** were prepared using a procedure similar to that described for **3a**. Selected spectroscopic and analytical data are listed for each compound.

Preparation of $[Fe_2(CO)_5(\mu\text{-PPh}_2)(\mu-\eta^1(C):\eta^2(C):\eta^1(N)\text{-}\{HC=C(NHCH_2Ph)CH_3\})]$ (3b). Obtained as deep red crys-

tals in 66% yield from dichloromethane/*n*-hexane at room temperature. IR (ν(CO), cm^{-1}, C_6H_{14}): 2029 m, 1984 s, 1959 s, 1928 m. $^{31}P\{^1H\}$ NMR (202.35 MHz, $CDCl_3$, 298 K, δ): 152.4 (s, μ-PPh_2). ^1H NMR (500.1 MHz, $CDCl_3$, 298 K, δ): 7.62−7.25 (m, 15H, C_6H_5), 4.85 (d, $^3J_{PH}$, 19.7 Hz, 1H, *H*C═CCH$_3$), 4.47 (dd, $^2J_{HH}$ = 13.5 Hz, $^3J_{HH}$ = 5.1 Hz, 1H, C*H*$_a$H$_b$Ph), 4.15 (dd, $^2J_{HH}$ = 13.5 Hz, $^3J_{HH}$ = 7.6 Hz, 1H, CH$_a$*H*$_b$Ph), 3.83 (br m, 1H, N−*H*), 2.39 (s, 3H, C═CC*H*$_3$). $^{13}C\{^1H\}$ NMR (125.65 MHz, $CDCl_3$, 298 K, δ): 219.7 (d, $^2J_{PC}$ = 16.5 Hz, CO), 214.5 (d, $^2J_{PC}$ = 11.0 Hz, CO), 140.5 (d, $^1J_{PC}$ = 28.9 Hz, C_6H_5), 139.1 (d, $^1J_{PC}$ = 33.0 Hz, C_6H_5), 135.2−127.8 (m, C_6H_5), 126.8 (d, $^2J_{PC}$ = 40.3 Hz, H*C*═CCH$_3$), 121.0 (s, C═*C*CH$_3$), 55.9 (s, *C*H$_2$-Ph), 23.3 (d, $^3J_{PC}$ = 8.2 Hz, C═C*C*H$_3$). Anal. Calcd for $C_{27}H_{22}Fe_2NO_5P$: C, 55.61; H, 3.80; N, 2.40. Found: C, 55.42; H, 3.77; N, 2.40.

Preparation of [Fe$_2$(CO)$_5$(μ-PPh$_2$)(μ−η^1(*C*):η^2(*C*):η^1(*N*)-{HC═C(NHC$_6$H$_{11}$)CH$_3$})] (3c). Isolated as red crystals in 54% yield from dichloromethane−*n*-hexane. IR (ν(CO), cm^{-1}, C_6H_{14}): 2027 m, 1981 s, 1957 s, 1927 m. $^{31}P\{^1H\}$ NMR (202.35 MHz, $CDCl_3$, 298 K, δ): 151.0 (s, μ-PPh_2). ^1H NMR (500.1 MHz, $CDCl_3$, 298 K, δ): 7.51−7.47 (m, 4H, C_6H_5), 7.21−7.05 (m, 6H, C_6H_5), 4.72 (d, $^3J_{PH}$, 20.2 Hz, 1H, *H*C═CCH$_3$), 3.62 (d, $^3J_{PH}$ = 9.8 Hz, 1H, N−*H*), 2.73 (m, 1H, N−C−*H*), 2.28 (s, 3H, C═CC*H*$_3$), 2.06−1.20 (m, Cy−C*H*$_2$, 10H). $^{13}C\{^1H\}$ NMR (125.65 MHz, $CDCl_3$, 298 K, δ): 220.7 (d, $^2J_{PC}$ = 17.0 Hz, CO), 214.6 (d, $^2J_{PC}$ = 2.7 Hz, CO), 210.2 (d, $^2J_{PC}$ = 11.3 Hz, CO), 140.7 (d, $^1J_{PC}$ = 27.9 Hz, C_6H_5), 139.3 (d, $^1J_{PC}$ = 33.5 Hz, C_6H_5), 133.1 (d, $^2J_{PC}$ = 8.8 Hz, C_6H_5), 132.6 (d, $^2J_{PC}$ = 8.8 Hz, C_6H_5), 129.3−127.8 (m, C_6H_5), 126.5 (d, $^2J_{PC}$ = 40.8 Hz, H*C*═CCH$_3$), 120.0 (s, C═*C*CH$_3$), 57.4 (s, Cy−*C*−N), 35.4 (s, Cy−*C*H$_2$), 34.6 (s, Cy-*C*′H$_2$), 25.7 (s, Cy−*C*″H$_2$), 24.7 (s, Cy−*C*‴H$_2$), 24.1 (s, Cy−*C*⁗H$_2$), 23.3 (s, C═C*C*H$_3$). Anal. Calcd for $C_{26}H_{26}Fe_2NO_5P$: C, 54.30; H, 4.56; N, 2.43. Found: C, 54.05; H, 4.42; N, 2.41.

Preparation of [Fe$_2$(CO)$_5$(μ-PPh$_2$)(μ−η^1(*C*):η^2(*C*):η^1(*N*)-{HC═C(NHCH$_2$CH$_2$CH$_3$)CH$_3$})] (3d). Isolated as red crystals in 70% yield from dichloromethane−*n*-hexane. IR (ν(CO), cm^{-1}, C_6H_{14}): 2027 m, 1982 s, 1957 s, 1928 m. $^{31}P\{^1H\}$ NMR (202.35 MHz, $CDCl_3$, 298 K, δ): 152.0 (s, μ-PPh_2). ^1H NMR (500.1 MHz, $CDCl_3$, 298 K, δ): 7.60−7.52 (m, 4H, C_6H_5), 7.33−7.25 (m, 6H, C_6H_5), 4.84 (d, $^3J_{PH}$, 19.8 Hz, 1H, *H*C═CCH$_3$), 3.50 (br d, $^3J_{PH}$ = 5.25 Hz, 1H, N−*H*), 3.29 (m, 1H, N−C*H*$_a$H$_b$-CH$_2$CH$_3$), 2.93 (m, 1H, N−CH$_a$*H*$_b$CH$_2$CH$_3$), 2.35 (s, 3H, C═CC*H*$_3$), 1.89 (m, 2H, N−CH$_2$C*H*$_2$CH$_3$), 1.08 (t, $^3J_{HH}$ = 7.5 Hz, 3H, N−CH$_2$CH$_2$C*H*$_3$). $^{13}C\{^1H\}$ NMR (125.65 MHz, $CDCl_3$, 298 K, δ): 220.8 (d, $^2J_{PC}$ = 17.0 Hz, CO), 214.5 (d, $^2J_{PC}$ = 3.0 Hz, CO), 209.8 (d, $^2J_{PC}$ = 11.1 Hz, CO), 140.7 (d, $^1J_{PC}$ = 27.9 Hz, C_6H_5), 139.1 (d, $^1J_{PC}$ = 34.1 Hz, C_6H_5), 133.1−127.8 (m, C_6H_5), 126.7 (d, $^2J_{PC}$ = 40.3 Hz, H*C*═CCH$_3$), 120.6 (s, C═*C*CH$_3$), 53.4 (s, N−*C*H$_2$CH$_2$CH$_3$), 23.2 (s, N−CH$_2$*C*H$_2$CH$_3$), 23.2 (s, C═C*C*H$_3$), 11.0 (s, N−CH$_2$CH$_2$*C*H$_3$). Anal. Calcd for $C_{23}H_{22}Fe_2NO_5P$: C, 51.63; H, 4.14; N, 2.62. Found: C, 51.92; H, 3.96; N, 2.61.

Transformation of 3a into [Fe$_2$(CO)$_5${P(OMe)$_3$}(μ-PPh$_2$)-(μ-CHC(CH$_3$){NHPr^i})] (4a). A toluene solution (30 mL) of complex **3a** (0.213 g, 0.4 mmol) and trimethyl phosphite (0.235 mL, 2.0 mmol) was heated at 67 °C for 2.5 h, during which time the reaction mixture turned from red-orange to deep red. The solvent was removed under reduced pressure to leave a red oily residue, which was dissolved in dichloromethane, absorbed onto deactivated alumina placed on a 30 × 300 mm column, and eluted with dichloromethane−*n*-hexane (50/50, v/v). A single major red band eluted, which was collected and crystallized from *n*-hexane to yield deep red crystals of **4a** in 65% yield (0.17 g). IR (ν(CO), cm^{-1}, C_6H_{14}): 2015 m, 1959 s, 1942 m, 1917 w. $^{31}P\{^1H\}$ NMR (202.35 MHz, $CDCl_3$, 298 K, δ): 187.4 (d, $^2J_{PP}$ = 44.5 Hz, μ-PPh_2), 146.0 (d, $^2J_{PP}$ = 44.5, $P(OMe)_3$). ^1H NMR (500.1 MHz, $CDCl_3$, 298 K, δ): 7.27−7.12 (m, 10H, C_6H_5), 3.69 (sept, $^3J_{HH}$ = 6.4 Hz, 1H, C*H*(CH$_3$)$_2$), 3.45 (d, $^3J_{PH}$ = 11.3 Hz, 9H, P(OC*H*$_3$)$_3$), 1.97 (s, 3H, C*H*$_3$), 1.46 (dd, $^3J_{PH}$ = 34.8 Hz, $^3J_{PH}$ = 3.2 Hz, 1H, μ-C*H*), 1.22 (d, $^3J_{HH}$ = 6.4 Hz, CH(C*H*$_3$)$_2$). $^{13}C\{^1H\}$ NMR (125.65 MHz, $CDCl_3$, 298 K, δ): 212.2 (dd, $^2J_{PC}$ = 12.3 Hz, CO), 215.0 (d, $^2J_{PC}$ = 20.0 Hz, $^2J_{PC}$ = 12.2 Hz, CO), 198.5 (d, $^3J_{PC}$ = 11.3 Hz, *C*═N), 142.1−127.1 (m, C_6H_5), 78.3 (br m, μ-*C*H), 51.4 (s, P(O*C*H$_3$)$_3$), 45.1 (s, *C*H(CH$_3$)$_2$), 23.0 (s, CH(*C*H$_3$)$_2$), 18.6 (s, *C*H$_3$). Anal. Calcd for $C_{26}H_{31}Fe_2NO_8P_2$: C, 47.38; H, 4.74; N, 2.12. Found: C, 47.53; H, 4.56; N, 2.09.

Compound **4c** was prepared using a procedure similar to that described for **4a**. Selected spectroscopic and analytical data are listed below.

Transformation of 3c into [Fe$_2$(CO)$_5${P(OMe)$_3$}(μ-PPh$_2$)-(μ-CHC(CH$_3$){NHCy})] (4c). Isolated as red crystals in 70% yield from *n*-hexane at room temperature. IR (ν(CO), cm^{-1}, C_6H_{14}): 2015 m, 1959 s, 1940 m, 1915 w. $^{31}P\{^1H\}$ NMR (202.35 MHz, $CDCl_3$, 298 K, δ): 187.6 (d, $^2J_{PP}$ = 47.0 Hz, μ-PPh_2), 146.1 (d, $^2J_{PP}$ = 47.0 Hz, $P(OMe)_3$). ^1H NMR (500.1 MHz, $CDCl_3$, 298 K, δ): 7.77−7.11 (m, 10H, C_6H_5), 3.44 (d, $^3J_{PH}$ = 11.3 Hz, 9H, P(OC*H*$_3$)$_3$), 3.30 (m, 1H, Cy−C$_\alpha$*H*), 1.97 (s, 3H, C*H*$_3$), 1.86 (br m, 1H, Cy−C′*H*), 1.72 (br, 1H, Cy−C″*H*), 1.55 (br m, 1H, Cy−C‴*H*), 1.48 (dd, $^3J_{PH}$ = 35.4 Hz, $^3J_{PH}$ = 3.7 Hz, 1H, μ-C*H*), 1.32−1.18 (m, 7H, Cy−*H*). $^{13}C\{^1H\}$ NMR (125.65 MHz, $CDCl_3$, 298 K, δ): 219.7 (s, CO), 218.0 (s, CO), 217.3 (dd, $^2J_{PC}$ = 13.1 Hz, $^2J_{PC}$ = 4.6 Hz, CO), 198.5 (d, $^3J_{PC}$ = 11.8 Hz, *C*═N), 142.1−127.0 (m, C_6H_5), 78.0 (br m, μ-*C*H), 54.9 (s, Cy−*C*−N), 51.5 (s, P(O*C*H$_3$)$_3$), 33.6 (s, Cy−*C*H$_2$), 32.5 (s, Cy−*C*′H$_2$), 25.1 (s, Cy−*C*″H$_2$), 24.7 (s, Cy−*C*‴H$_2$), 24.1 (s, Cy−*C*⁗H$_2$), 19.0 (s, −C*C*H$_3$). Anal. Calcd for $C_{29}H_{35}Fe_2NO_8P_2$: C, 49.81; H, 5.05; N, 2.00. Found: C, 49.85; H, 4.97; N, 1.98.

Preparation of [Fe$_2$(CO)$_5${P(OMe)$_3$}(μ-PPh$_2$){μ-O═C−CH═CMe(NHPr^i)}] (5a). A toluene solution (20 mL) of **2a** (0.226 g, 0.4 mmol) and trimethyl phosphite (0.047 mL, 0.4 mmol) was heated at reflux for 1 h, resulting in a color change from orange to red. The solvent was removed under reduced pressure and the red oily residue dissolved in dichloromethane, absorbed onto deactivated alumina, placed on a 30 × 300 mm column, and eluted with dichloromethane−*n*-hexane (40/60, v/v). A single major orange band eluted which was collected and crystallized from *n*-hexane to yield orange-red crystals of **5a** in 62% yield (0.170 g). IR (ν(CO), cm^{-1}, C_6H_{14}): 2035 s, 1982 s, 1975 s, 1948 m. $^{31}P\{^1H\}$ NMR (202.35 MHz, $CDCl_3$, 298 K, δ): 178.2 (d, $^2J_{PP}$ = 62.0 Hz, μ-PPh_2), 171.1 (d, $^2J_{PP}$ = 62.0 Hz, $P(OMe)_3$). ^1H NMR (500.1 MHz, $CDCl_3$, 298 K, δ): 8.41 (d, $^2J_{HH}$ = 8.6 Hz, 1H, N−*H*), 7.76−7.02 (m, 10H, C_6H_5), 5.01 (s, 1H, O═CC*H*), 3.64 (d, $^3J_{PH}$ = 11.0 Hz, 9H, P(OC*H*$_3$)$_3$), 3.25 (sept, $^3J_{HH}$ = 6.1 Hz, 1H, C*H*(CH$_3$)$_2$), 1.68 (s, 3H, C*H*$_3$), 0.87 (d, $^3J_{HH}$ = 6.1 Hz, 3H, C*H*(CH$_3$)$_2$), 0.69 (d, $^3J_{HH}$ = 6.1 Hz, 3H, C*H*(CH$_3$)$_2$). $^{13}C\{^1H\}$ NMR (125.65 MHz, $CDCl_3$, 298 K, δ): 258.2 (dd, $^3J_{PC}$ = 19.6 Hz, $^3J_{PC}$ = 3.5 Hz, μ-*C*═O), 218.1 (dd, $^2J_{PC}$ = 15.0 Hz, $^2J_{PC}$ = 16.0 Hz, CO), 217.0 (br, CO), 214.9 (br, CO), 214.8 (dd, $^2J_{PC}$ = 19.6 Hz, $^2J_{PC}$ = 16.0, CO), 152.0 (s, *C*═N), 141.0−127.3 (m, C_6H_5), 113.4 (s, HCC═O), 51.8 (d, $^2J_{PC}$ = 3.6 Hz, P(O*C*H$_3$)$_3$), 44.3 (s, *C*H(CH$_3$)$_2$), 23.5 (s, CH(*C*H$_3$)$_2$), 23.4 (s, CH(*C*H$_3$)$_2$), 17.7 (s, *C*H$_3$). Anal. Calcd for $C_{27}H_{31}Fe_2NO_9P_2$: C, 47.19; H, 4.55; N, 2.04. Found: C, 47.24; H, 4.51; N, 2.01.

Preparation of [Fe$_2$(CO)$_5${P(OMe)$_3$}(μ-PPh$_2$){μ-O═C−CH═CMe(NHCH$_2$Ph)}] (5b). Prepared using a procedure similar to that described for **5a**. Isolated as orange crystals in 70% yield from dichloromethane−*n*-hexane. IR (ν(CO), cm^{-1}, C_6H_{14}): 2036 s, 1984 s, 1975 s, 1948 m. $^{31}P\{^1H\}$ NMR (202.35 MHz, $CDCl_3$, 298 K, δ): 178.1 (d, $^2J_{PP}$ = 62.0 Hz, μ-PPh_2), 170.7 (br d, $^2J_{PP}$ = 62.0 Hz, $P(OMe)_3$). ^1H NMR (500.1 MHz, $CDCl_3$, 298 K, δ): 8.76 (br s, 1H, N−*H*), 7.75−6.76 (m, 15H, C_6H_5), 5.21 (s, 1H, O═CC*H*), 3.96 (s, 2H, C*H*$_2$Ph), 3.45 (d, $^3J_{PH}$ = 9.5 Hz, 9H, P(OC*H*$_3$)$_3$), 1.57 (s, 3H, C*H*$_3$). $^{13}C\{^1H\}$ NMR (125.65 MHz, $CDCl_3$, 298 K, δ): 261.5 (dd, $^3J_{PC}$ = 18.3 Hz, $^3J_{PC}$ = 1.8 Hz, μ-*C*═O), 218.2 (d, $^2J_{PC}$ = 13.7 Hz, CO), 217.0 (br, CO), 214.9 (dd, $^2J_{PC}$ = 14.1 Hz, CO), 153.2 (s, *C*═N), 141.0−127.0 (m, C_6H_5), 114.3 (s, HCC═O), 51.8 (s, $P(OMe)_3$), 46.8 (s, *C*H$_2$Ph), 18.3 (s, *C*H$_3$). Anal. Calcd for $C_{31}H_{31}Fe_2NO_9P_2$: C, 50.64; H, 4.25; N, 1.91. Found: C, 50.58; H, 4.13; N, 1.87.

Table 5. Summary of Crystal Data and Structure Determination for Compounds 2a, 3a, 4c, 5a, and 5b

	2a	3a	4c	5a	5b
mol form	$C_{24}H_{22}Fe_2NO_6P$	$C_{23}H_{22}Fe_2NO_5P$	$C_{29}H_{35}Fe_2NO_8P_2$	$C_{27}H_{31}Fe_2NO_9P_2$	$C_{31}H_{31}Fe_2NO_9P_2$
fw	563.1	535.1	699.2	687.2	735.2
cryst size, mm	0.71 × 0.34 × 0.12	0.43 × 0.21 × 0.17	0.67 × 0.20 × 0.10	0.62 × 0.38 × 0.08	0.46 × 0.25 × 0.17
cryst syst	monoclinic	triclinic	monoclinic	triclinic	monoclinic
space group	$P2_1/c$	$P\bar{1}$	$P2_1/n$	$P\bar{1}$	$P2_1/n$
a, Å	9.6682(6)	9.5587(5)	9.7469(9)	10.0308(10)	10.8823(9)
b, Å	13.6423(8)	9.6539(5)	18.4631(17)	11.2292(12)	17.4228(16)
c, Å	19.5172(11)	14.4450(8)	17.6850(16)	15.5243(16)	17.4497(15)
α, deg		76.017(2)		88.880(3)	
β, deg	103.548(2)	83.793(2)	94.799(2)	71.599(3)	96.957(3)
γ, deg		63.853(2)		67.426(3)	
V, Å^3	2502.6(3)	1161.10(11)	3171.4(5)	1521.8(3)	3284.1(5)
Z	4	2	4	2	4
D_{calcd}, g cm^{-3}	1.495	1.530	1.464	1.500	1.487
μ, mm^{-1}	1.262	1.352	1.064	1.110	1.034
$F(000)$	1152	548	1448	708	1512
θ range, deg	2.15−28.88	2.37−28.88	1.60−28.80	1.98−25.00	2.10−28.76
max indices h,k,l	12, 18, 25	12, 12, 18	12, 23, 23	11, 13, 18	14, 22, 23
no. of reflns measd	15 899	8846	19 852	9021	12 326
no. of unique reflns	5995	5328	7401	5269	6009
no. of reflns with $F^2 > 2\sigma(F^2)$	4899	4853	4990	3403	4459
transmission coeff range	0.682−0.862	0.734−0.894	0.649−0.831	0.428−0.894	0.652−0.831
R_{int} (on F^2)	0.0279	0.0163	0.0427	0.0538	0.0362
weighting params[a] a, b	0.0365, 1.1936	0.0485, 1.0883	0.0596, 0	0.1173, 0	0.0452, 0.8649
R[b]	0.0364	0.0400	0.0458	0.0759	0.0387
R_w[c]	0.0855	0.0995	0.1134	0.1960	0.0940
GOF[d] on F^2	1.043	1.072	0.989	0.956	1.004
max, min in diff map, e Å^{-3}	0.52, −0.39	1.06, −0.60	0.79, −0.44	2.88, −1.52	0.56, −0.29

[a] $w^{-1} = \sigma^2(F_o^2) + (aP)^2 + bP$, where $P = (F_o^2 + 2F_c^2)/3$. [b] Conventional $R = \sum||F_o| - |F_c||/\sum|F_o|$ for "observed" reflections having $F_o^2 > 2\sigma(F_o^2)$. [c] $R_w = [\sum w(F_o^2 - F_c^2)^2/\sum w(F_o^2)^2]^{1/2}$ for all data. [d] GOF $= [\sum w(F_o^2 - F_c^2)^2/(\text{no. of unique reflns} - \text{no. of params})]^{1/2}$.

Carbonylation of [$Fe_2(CO)_5${$P(OMe)_3$}(μ-PPh_2)(μ-CHC(CH_3){$NHPr^i$})] (4a). A toluene solution of **4a** (0.150 g, 0.2 mmol) was heated at 80 °C for 3 h while maintaining a gentle purge of carbon monoxide through the reaction mixture. The solvent was removed under reduced pressure to leave a red oily residue, which was dissolved in a minimum volume of dichloromethane and absorbed onto alumina. Elution with dichloromethane−*n*-hexane (60/40, v/v) gave two separate products. The first band to elute was obtained as a red-orange unidentified oil. The slower moving fraction was characterizd as **5a** by comparison of its spectroscopic properties with those of an authentic sample prepared earlier. Concentration and subsequent cooling of this fraction gave yellow crystals of **5a** in 35% yield (0.054 g, 0.07 mmol).

Crystal Structure Determination of 2a, 3a, 4c, 5a, and 5b. All measurements were made on a Bruker AXS SMART CCD area-detector diffractometer at 160 K, using Mo Kα radiation (λ = 0.710 73 Å) and narrow frame exposures (0.3° in ω). Cell parameters were refined from the observed ω angles of all strong reflections in each data set. Intensities were corrected semiempirically for absorption, based on symmetry-equivalent and repeated reflections. No significant intensity decay was observed. Extinction effects were negligible. The structures were solved by direct methods and refined on F^2 values for all unique data by full-matrix least squares. Table 5 gives further details. All non-hydrogen atoms were refined anisotropically. H atoms, located in difference maps, were constrained with a riding model except for those attached to C(1) and N(1) in **3a** and C(1) in **4c**, which were refined freely because of the nonstandard geometry; U(H) was set at 1.2 (1.5 for methyl groups) times U_{eq} for the parent atom. Programs used were SHELXTL[38a] for structure solution, refinement and molecular graphics, Bruker AXS SMART (control), and SAINT (integration) and local programs.[38b]

Acknowledgment. We thank the University of Newcastle upon Tyne for financial support, the Nuffield Foundation and The Royal Society for grants (S.D.), and the EPSRC for funding for a diffractometer (W.C.). Many thanks are due to reviewer 67 for some thought-provoking and informative comments.

Supporting Information Available: Tables of the structure determination (Tables S1, S6, S11, S16, and S21), non-hydrogen atomic positional parameters (Tables S2, S7, S12, S17, and S22), full bond distances and angles (Tables S3, S8, S13, S18, and S23), anisotropic displacement parameters (Tables S4, S9, S14, S19, and S24), and hydrogen atomic coordinates (Tables S5, S10, S15, S20, and S25) for **2a**, **3a**, **4c**, **5a**, and **5b** (29 pages). Ordering information is given on any current masthead page. Observed and calculated structure factor tables are available from the authors upon request.

OM980108B

(38) (a) Sheldrick, G. M. *SHELXTL user manual, version 5*; Bruker AXS Inc.: Madison, WI, 1994. (b) *SMART and SAINT software for CCD diffractometers*; Bruker AXS Inc.: Madison, WI, 1994.